Quaternary Science Reviews 132 (2016) 40–56

Contents lists available at ScienceDirect

Quaternary Science Reviews

journal homepage: www.elsevier.com/locate/quascirev

A cosmogenic ^{3}He chronology of late Quaternary glacier fluctuations in North Island, New Zealand (39°S)

Shaun R. Eaves [a, b, *], Andrew N. Mackintosh [a, b], Gisela Winckler [c], Joerg M. Schaefer [c], Brent V. Alloway [b], Dougal B. Townsend [d]

[a] Antarctic Research Centre, Victoria University of Wellington, P.O. Box 600, Wellington 6140, New Zealand
[b] School of Geography Environment and Earth Sciences, Victoria University of Wellington, P.O. Box 600, Wellington 6140, New Zealand
[c] Lamont-Doherty Earth Observatory of Columbia University P.O. Box 1000, Palisades, NY 10964, USA
[d] GNS Science, P.O. Box 30-368, Lower Hutt 5040, New Zealand

ARTICLE INFO

Article history:
Received 24 March 2015
Received in revised form
3 November 2015
Accepted 4 November 2015
Available online 28 November 2015

Keywords:
Cosmogenic ^{3}He
Last Glacial Maximum
Last glacial cycle
Equilibrium line altitude
Tephrostratigraphy
New Zealand
Southern Hemisphere

ABSTRACT

Mountain glaciers advance and retreat primarily in response to changes in climate. Establishing the timing and magnitude of mountain glacier fluctuations from geological records can thus help to identify the drivers and mechanisms of past climate change. In this study, we use cosmogenic ^{3}He surface exposure dating and tephrochronology to constrain the timing of past glaciation on Tongariro massif in central North Island, New Zealand (39°S). Exposure ages from moraine boulders show that valley glaciation persisted between c. 30–18 ka, which coincides with the global Last Glacial Maximum. Reinterpretation of moraine tephrostratigraphy, using major element geochemistry analysis, shows that ice retreat and climatic amelioration at the last glacial termination was well underway prior to 14 ka. The equilibrium line altitude in central North Island, during the Last Glacial Maximum, was c. 1400–1550 m above sea level, which is c. 930–1080 m lower than present. Considering the uncertainties in the glacial reconstruction and temperature lapse rates, we estimate that this equilibrium line altitude lowering equates to a temperature depression of 5.6 ± 1.1 °C, relative to present. Our mapping and surface exposure dating also show evidence for an earlier period of glaciation, of similar magnitude to the Last Glacial Maximum, which culminated prior to 57 ka, probably during Marine Isotope Stage 4. Good agreement between the timing and magnitude of glacier fluctuations in central North Island and the Southern Alps indicate a response to a common climatic forcing during the last glacial cycle.

1. Introduction

Explaining the drivers of Quaternary climate cycles in the Southern Hemisphere remains an outstanding goal of palaeoclimate research. New Zealand is one of the few locations in the Southern Hemisphere where terrestrial palaeoclimate can be reconstructed. Furthermore, it is ideally situated to record fluctuations of the southern westerly winds and the oceanic subtropical and subpolar fronts (Fig. 1), which are considered to have played an important role in past climate dynamics (Denton et al., 2010). Regional tectonic uplift and localised effusive volcanism have resulted in high-elevation and high-relief topography in both the North and South Island of New Zealand, which support contemporary glaciers spanning latitudes from 39°S to 46°S. Empirical and model-based analyses show contemporary glacier mass balance in New Zealand is most sensitive to changes in atmospheric temperature (Oerlemans, 1997; Anderson and Mackintosh, 2006; Anderson et al., 2010; Brook et al., 2011). Steep mass balance gradients and relatively high ice velocities mean that mass balance changes are translated to the termini of mountain glaciers over timescales of 10^{1}–10^{2} yrs (Oerlemans, 1997; Purdie et al., 2014). Geological records of past glacier fluctuations in New Zealand therefore represent an important proxy for past climatic change in the southern mid-latitudes (e.g. Anderson and Mackintosh, 2006; Schaefer et al., 2006, 2009; Kaplan et al., 2010, 2013; Putnam et al., 2010a, 2012, 2013a, 2013b; Golledge et al., 2012; Barrows et al., 2013; Doughty et al., 2013; Rother et al., 2014).

Existing reconstructions of late Quaternary glacier fluctuations in New Zealand have predominantly concentrated on large outlet

* Corresponding author. Antarctic Research Centre, Victoria University of Wellington, P.O. Box 600, Wellington 6140, New. Zealand.
E-mail address: shaun.eaves@vuw.ac.nz (S.R. Eaves).

http://dx.doi.org/10.1016/j.quascirev.2015.11.004
0277-3791/

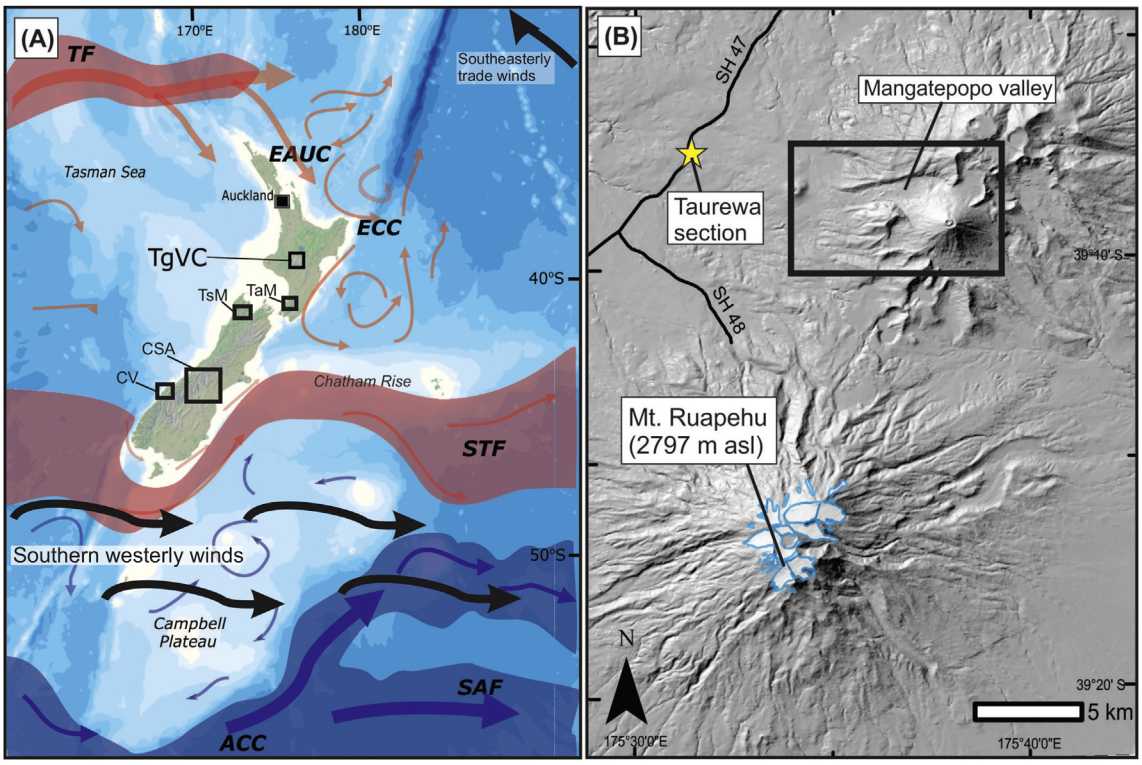

Fig. 1. (A) Contemporary general atmospheric and oceanic circulation in New Zealand and locations of sites referred to in text (background image sourced from National Institute for Water and Atmospheric research (NIWA)). Sites: TgVC = Tongariro Volcanic Centre; TaM = Tararua Mts.; TsM = Tasman Mts.; CSA = Central Southern Alps; CV = Cascade valley. Ocean currents: EAUC = East Australian Current; ECC = East Cape Current; STF = Sub-tropical front; SAF = Sub-Antarctic Front; ACC = Antarctic Circumpolar Current; (B) Hill-shaded digital elevation model (Columbus et al., 2011) of the Tongariro massif and Mt. Ruapehu, with the main study region defined (black outline). The location of proximal tephra reference site at Taurewa and Mt. Ruapehu glacier outlines according to Keys (1988) are also shown.

glaciers that drained the central Southern Alps (e.g. Porter, 1975; Suggate and Almond, 2005; Schaefer et al., 2006; Barrows et al., 2013; Putnam et al., 2013b; Rother et al., 2014). Radiocarbon and luminescence dating of peat and loess units, interbedded with glacial till and glaciofluvial outwash, have provided a broad chronostratigraphic framework for this region (Suggate, 1990; Suggate and Almond, 2005). More recently, cosmogenic surface exposure dating of moraine boulders has provided the means to directly constrain the timing and magnitude of past glacier fluctuations (Schaefer et al., 2006; Barrows et al., 2013; Putnam et al., 2013a, b; Rother et al., 2014). During the last glacial cycle, glacier length in the Southern Alps peaked relatively early (c. 32–26 ka; Suggate and Almond, 2005; Putnam et al., 2013b; Barrows et al., 2013; Rother et al., 2014), in comparison to global ice volume (Clark et al., 2009). At this time, local equilibrium line altitudes were depressed by c. 850 m and temperatures were c. 6–6.5 °C colder, relative to present (Golledge et al., 2012). Subsequently, glaciers fluctuated about these positions until at least c. 18 ka before rising temperatures resulted in widespread deglaciation (Schaefer et al., 2006; Putnam et al., 2013a, b; Rother et al., 2014). Recent work has shown that advances of former outlet glaciers in central Southern Alps, prior to the Last Glacial Maximum (LGM), culminated at 42 ± 1 ka (Kelley et al., 2014), 65 ± 3 ka (Schaefer et al., 2015) and 139 ± 11 ka (Putnam et al., 2013b). Previous research had suggested the occurrence of significant pre-LGM glacial advances in New Zealand (Williams, 1996; Almond et al., 2001; Preusser et al., 2005; Sutherland et al., 2007; McCarthy et al., 2008), but the exact timing of these events was poorly resolved due to low chronological precision or small sample populations.

Resolving the timing and magnitude of late Quaternary glacier fluctuations in locations outside of the central Southern Alps will provide insight to the synchroneity and climatic gradients of past climate change in the southern mid-latitudes. In this study, we use cosmogenic ^{3}He exposure dating, tephrochronology and equilibrium line altitude (ELA) reconstruction techniques, to provide the first direct age constraint on the timing and magnitude of glacier fluctuations on Tongariro massif, central North Island (39°S).

2. Setting

2.1. Regional climatic situation

Situated between 34°S and 47°S in the south west sector of the Pacific Ocean, New Zealand spans subtropical and subpolar climes (Fig. 1). Westerly atmospheric circulation dominates between 30°S and 60°S and is responsible for the eastward migrating troughs and anticyclones that define weather variability in New Zealand year-round (Sturman and Tapper, 1996). Interception of such weather systems by the predominantly NE–SW trending axial ranges results in a distinct zonal precipitation gradient. Meanwhile, interannual to interdecadal air temperature anomalies in New Zealand are strongly influenced by upwind sea surface temperatures (Sutton et al., 2005). The latitudinal range and high topographic relief of the New Zealand landmass result in meridional and zonal gradients in air temperature and precipitation respectively. Contemporary oceanic influences on North Island, New Zealand (34–41°S) are largely sub-tropical, predominantly originating from an eastward flowing branch of the equatorial-sourced East Australian Current, known as the Tasman Front, which descends the northeast coast before continuing eastwards along the northern margin of the Chatham Rise (Fig. 1). In contrast, South Island (40–47°S) intersects the sub-tropical front (STF), where sub-tropical gyres and sub-

Antarctic water masses converge, representing a temperature, salinity and nutrient boundary, which defines the northern margin of the Southern Ocean (Sikes et al., 2009). Consequently, steep zonal and meridional sea surface temperature (SST) gradients exist across the New Zealand region (Uddstrom and Oien, 1999).

2.2. Study site and previous work

Tongariro massif in central North Island (39.13°S, 175.65°E) forms part of Tongariro Volcanic Centre (TgVC; Fig. 1), which is an area of andesitic volcanism at the southwestern end of Taupo Volcanic Zone. Tongariro massif comprises c. 17 coalescing volcanic vents, with ages ranging from c. 270 ka to present (Hobden et al., 1996). The local climate, as recorded at Whakapapa village (1097 m asl) located 8 km SSW of our study site, is characterised by low seasonal precipitation variability, with total annual precipitation averaging c. 2800 mm (AD1981–2010; NIWA, 2014). Monthly mean temperatures at this station range from c. 13 °C in February to c. 3 °C in July, with an annual average of 7.5 °C (NIWA, 2014).

Geomorphological evidence for past glaciation on Tongariro massif has long been recognised (Mathews, 1967; Topping, 1974), however lack of chronological constraint has so far precluded any palaeoclimatic interpretation. Mathews (1967) first described conspicuous, lateral moraines in several valleys radiating from the volcano and correlate these landforms to the late Pleistocene moraines of the Southern Alps, based on their size and degree of preservation. Topping and Kohn (1973) identified two rhyolitic beds in a soil section overlying a large lateral moraine in the Mangatepopo valley, on the western side of Tongariro massif (Fig. 1). Using analyses of titano-magnetite assemblages, they correlated the lower bed to the Rerewhakaaitu Tephra (c. 17.5 ± 0.5 ka BP – Lowe et al., 2013), which is sourced from Okataina Volcanic Centre (OVC), situated c. 130 km north of Tongariro massif. This finding was then used to stratigraphically correlate the upper bed to the Waiohau Tephra (cf. Donoghue et al., 1995), also sourced from the OVC, at 14.0 ± 0.2 ka (Lowe et al., 2013). On the eastern flanks of Tongariro massif, Cronin and Neall (1997) identified both the Waiohau and Rerewhakaaitu Tephras at the base of soils overlying lateral moraines. These stratigraphic constraints provide minimum ages for the underlying moraines.

On nearby Mt. Ruapehu (2797 m asl), situated c. 15 km to the south west of Tongariro massif (Fig. 1), McArthur and Shepherd (1990) identify large lateral moraines in several valleys, which descend to an altitude of c. 1200 m asl. They suggest the former ice mass existed during the Last Glacial Maximum, based on the presence of the Kawakawa/Oruanui Tephra (25.4 ± 0.2 ka – Vandergoes et al., 2013), which is found interbedded within moraine-bound glaciolacustrine deposits.

2.2.1. Mangatepopo valley

The Mangatepopo valley is c. 6 km long and 1–2 km wide, with small, westward-flowing under-fit streams draining both the northern and southern valley margins, which converge at the valley mouth to form the Mangatepopo Stream (Fig. 2). Mangatepopo Stream then flows northwards, before forming a tributary of the Whanganui River, which is a major drainage channel for eastern-central North Island.

At the head of the Mangatepopo valley, South Crater is a large bedrock amphitheatre, which is 1 km across at its widest point and 250 m deep (Fig. 2; Fig. 3a). At 1967 m asl, Mt. Tongariro forms the highest point on the south-facing back wall of South Crater, while the Holocene-aged volcanic cone of Mt. Ngauruhoe (2287 m asl) is situated c. 3 km to the south. Following Mathews (1967), we interpret South Crater as a glacial cirque that served as the main accumulation centre for the former Mangatepopo glacier. The flat-bottomed, cirque floor is c. 1700 m asl, although this contemporary elevation represents infilling by an unknown thickness of post-glacial volcanic products. Bedrock spurs forming the mouth of the cirque have been partially overprinted by post-glacial lavas sourced from Mt. Ngauruhoe, however these spurs clearly curve towards the southwest, which indicates the direction of ice flow from this former accumulation zone.

To the southwest of Mt. Tongariro peak, the outer, western-facing slopes of South Crater exhibit a stacked sequence of truncated lava flows in a steep, concave amphitheatre, which is suggestive of headward erosion by a westward-flowing glacier. Field investigations show that bedrock exposures in this region exhibit glacially-polished surfaces, indicative of glacial abrasion by a temperate ice-mass (Fig. 2). Several radiometric (K/Ar) ages from lavas show that cone-building in the South Crater region occurred c. 70–100 ka (Hobden et al., 1996). These dates provide a maximum bracketing age for the creation of the erosional glacial landforms.

The surface of the main valley floor is convex, representing post-glacial infilling by lava flows and pyroclastics from the nearby volcanic vents. Both valley sides exhibit truncated lava cliffs, aligned parallel to the west-east trending valley axis, and are interpreted as having been eroded by ice. On the northern edge of Pukekaikiore (Fig. 2A), two such vertical cliffs are stacked on top of one another, separated by a clear bench, perhaps indicative of multiple erosive periods by ice masses of differing thickness. K/Ar dates from Pukekaikiore lavas range between c. 200–100 ka (Hobden et al., 1996), which suggests that the glacial erosion occurred during the last glacial cycle.

Multiple lateral moraines exist on both valley sides and can be differentiated chronologically, based on morphostratigraphic criteria. This distinction is clearest on the lower portion of the northern valley side where two large lateral moraines have significantly different crest heights and widths. Topographic profiles, aligned perpendicular to the moraine crest orientation illustrate the differing morphologies of these landforms (Fig. 2B). The outer moraine (M3) is c. 20 m tall, with a highly rounded crest, while the inner moraine (M2) is sharp-crested and significantly taller. We interpret these geomorphic differences as representing a considerable time gap between the two moraine forming glacial episodes, with the outer, older moraine (M3) having undergone a greater amount of degradation.

The lower portions (< 1200 m asl) of both M2 and M3 moraines have continuous coverage by palaeosols, interbedded with tephra and volcanic loess accumulation (Fig. 2; Fig. 3d,e). Between 1200 and 1250 m asl, these coverbeds become discontinuous, with the transitions from bare moraine to the coverbeds marked by erosional scarps, which indicate former, more extensive coverage of the moraine surface at this elevation. The upstream end of moraine M2 (>1250 m asl) is characterised by continuous thin (<1 m) coverbeds on the lower moraine slope, which thins towards the bare, rocky moraine crest (Fig. 3e). No erosional scarps exist on the upper portion of this moraine.

Directly upstream from moraine M2, moraine M1 is a single, continuous ridge (Fig. 3c), separated from M2 by a cliff, which represents the downstream limit of an underlying lava flow dated by Hobden et al. (1996) to 110 ± 6 ka. There is no tephra cover on M1 present today, nor are there any remnants to suggest that coverbeds have been more extensive in the past. It is likely that the greater elevation of M1 prevents any accumulation of fine-grained sediment due to wind exposure and lack of vegetation.

On the southern valley side, a single, sharp-crested lateral moraine extends westwards for c. 1 km, from Pukekaikiore (Fig. 2). The crest of this moraine is c. 40 m above the present day valley floor. Immediately down valley, two left latero-frontal moraines further constrain the former glacier margin. Soil and tephra cover

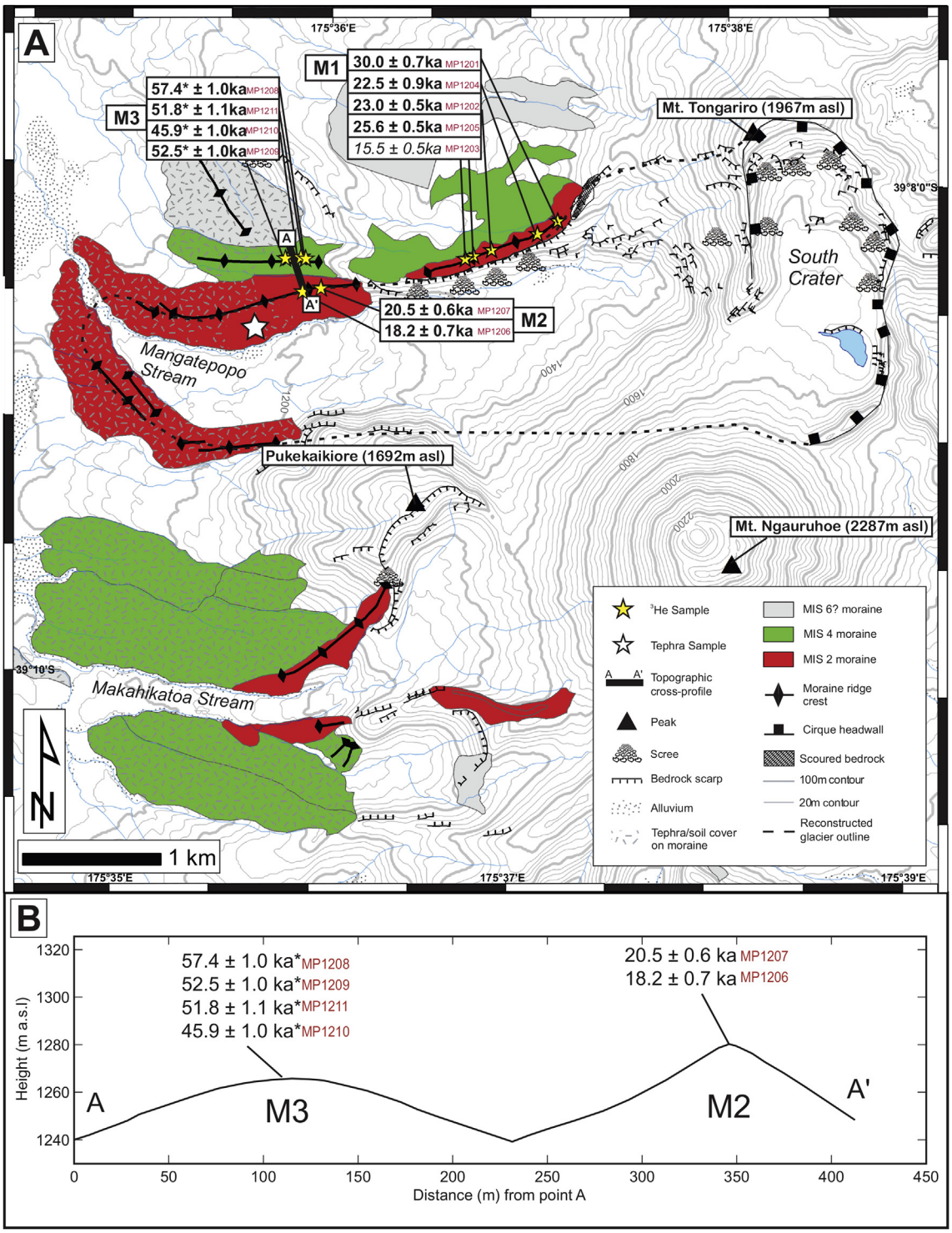

Fig. 2. (A) Glacial geomorphology and chronology of western Tongariro massif. Yellow stars represent the location of moraine boulder samples for cosmogenic ^{3}He exposure dating. Associated labels are the calculated exposure ages (an internal unceratinties), using 'Lm' scaling – see text for detailed description of age calculation methods. (B) Topographic profiles across moraines M2 and M3, with ^{3}He exposure ages and sample numbers. Note the greater roundness of the older, M3 crest. *Exposure ages for M3 are considered minimum ages for moraine formation – see text.

on these moraines precludes sampling for surface exposure dating, although both landforms exhibit relatively sharp crests, which suggests that they correlate with the M2 moraine on th eopposite valley side. The innermost moraines on both valley sides converge downstream at c. 1150 m asl, forming the valley mouth, thereby defining the maximum limit of the most recent period of valley glaciation (Fig. 3d).

2.2.2. *Makahikatoa Stream*

To the south of Mangatepopo valley, the northern headwaters of the Makahikatoa stream drain southwestwards from a northeast-southwest orientated bedrock amphitheatre, interpreted as a

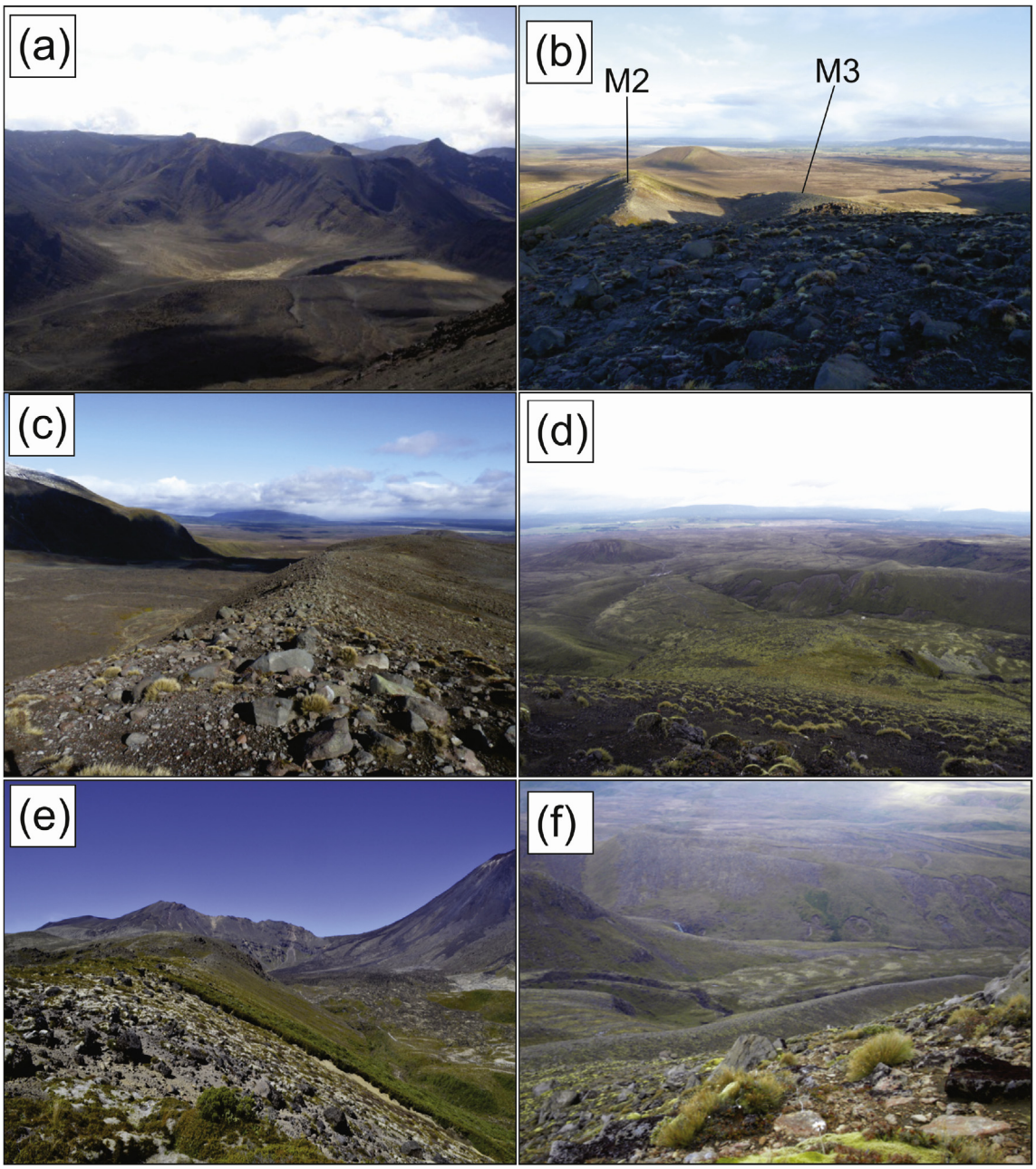

Fig. 3. (a) South Crater cirque, viewed from the upper slopes of Mt. Ngauruhoe; (b) moraines M2 (middle ground, left) and M3 (middle ground, centre), note the difference in morphometry between the two landforms; (c) a view down valley from the upstream end of moraine M1 – note the glacially truncated side of Pukekaikiore in shadow on the far valley side; (d) the inner lateral moraines of Mangatepopo valley clearly depict the former glacier terminus (photo taken from the upper western slopes of Pukekaikiore); (e) coverbeds on the ice-proximal flank of M2 moraine thin towards the crest; (f) the sharp-crested right lateral moraine of the Makahikatoa valley runs diagonally from left to right across this image (photo taken from the upper northern slopes of Pukekaikiore).

glacially eroded cliffs cut into the south-east flank of Pukekaikiore (Fig. 2). The eastern limits of this former glacial catchment are ill-defined owing to the Holocene lava flows of Mt. Nguaruhoe, which is situated immediately to the east.

A sharp-crested lateral moraine extends from the southern flank of Pukekaikiore, descending in a southwest direction for c. 500 m, terminating at c. 1275 m asl (Fig. 2). This moraine is paired by a shorter moraine ridge, issuing from a steep bedrock spur that defines the southern margin of this former glacial catchment. The right lateral moraine cross-cuts a significantly wider, more rounded moraine ridge that can be traced down valley to c. 1200 m asl and represents a significantly older glacial limit. Based on the morphostratigraphic relationship of these moraines, and their similarity in form to the moraines in Mangatepopo valley, we correlate them to the outer (M3) and inner (M1/M2) moraine ridges in Mangatepopo valley, respectively (Fig. 2).

3. Methods

3.1. Cosmogenic surface exposure dating

Moraine boulder samples were collected using a portable rock saw fitted with a segmented, diamond-tipped blade (e.g. Suganuma et al., 2012). Samples were only taken from boulders on the

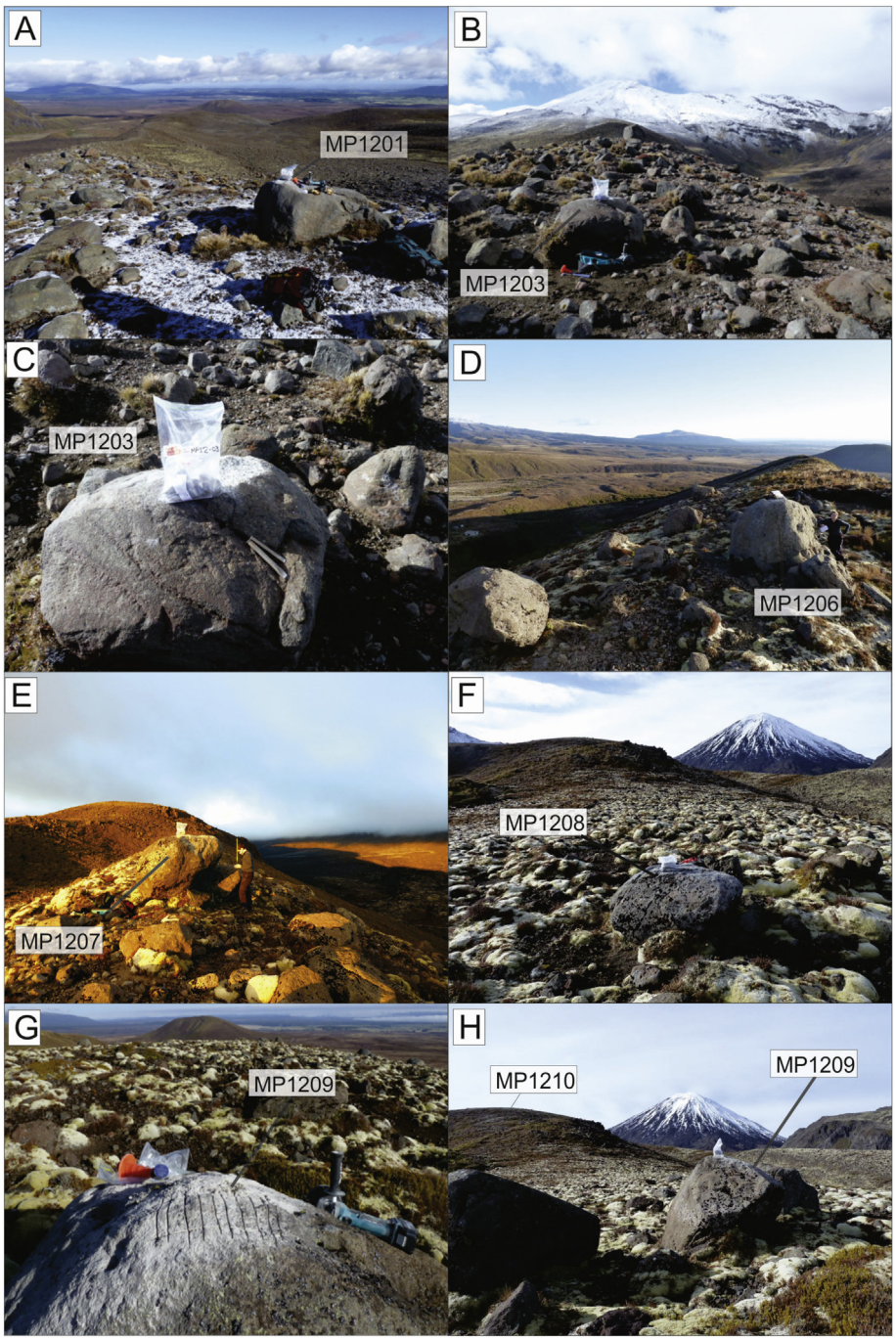

Fig. 4. Examples of boulders sampled for cosmogenic ^{3}He surface exposure dating. Visible sample bags denote sample position on boulder surface. (A) Sample MP1201 at the eastern end of moraine M1. Photo facing westwards. (B) Sample MP1203 on moraine M1 in the foreground, with Mt. Tongariro (1963 m asl) in the background. Photo facing northeast. (C) Fracturing on sample MP1203. (D) MP1206 on moraine M2. Note prominent lateral moraines on opposite valley side. Photo facing southwest. (E) MP1207 on moraine M2. Photo facing east. (F) Sample MP1208 on moraine M3. Note the highly diffuse moraine crest, compared to moraine M1. Also, note the Holocene cone of Mt. Ngauruhoe (background right). Photo facing east. (G) Weathered surface of sample MP1209. (H) Samples MP1209 and MP1210 on moraine M3. Photo facing east.

moraine crest (Fig. 4), and those close to known faults and beneath lava cliffs were avoided. Where possible, we sampled boulders that were partially embedded in the moraine matrix to minimise the likelihood that the boulder has undergone post-depositional rotation. All samples were collected from the highest point of the parent boulder, and all boulders were over 0.6 m tall, thus minimising the potential for past burial by snow and/or volcanic ash. Sampled boulder surfaces exhibited <12° dip relative to horizontal, thereby avoiding self-shielding. Azimuthal inclinations were measured in the field using a compass and clinometer and geometric shielding corrections were computed using the CRONUS-EARTH calculator (available at: http://hess.ess.washington.edu). All shielding corrections were less than 1% (Table 1). Sample locations and elevations were recorded using a Trimble GeoXH global positioning system, relative to the WGS84 datum. These data were differentially corrected using continuous measurements from GeoNet 'Chateau Observatory' ('VGOB') base station (39.20°S, 175.54°E; 1161 m asl), located 8 km south west of Mangatepopo

valley. Horizontal and vertical post-processed uncertainties for individual sample locations are <1 m.

Whole rock samples were jaw-crushed, rinsed in de-ionised water, and then dry-sieved to isolate the 250–500 μm size fraction. Density (>3.1 g cm^{-3}) and magnetic techniques were used to separate 150–600 mg of clinopyroxene (pigeonite). Crushing and mineral separation were undertaken using facilities at Victoria University of Wellington. Pyroxene separates were then prepared according to Bromley et al. (2014) at the Cosmogenic Nuclide Laboratory of Lamont-Doherty Earth Observatory (LDEO). Mineral separates were first leached in 5% hydrofluoric (HF)/2% nitric (HNO_3) acid solution for 24 h to remove adhering ground mass particles, followed by a separate 10% hydrochloric (HCl) acid solution for 24 h. Leached pyroxenes were visually inspected for purity and wrapped in aluminium foil.

Each sample was completely degassed by heating in a furnace to >1300 °C for 15 min, during which, released gases were exposed to a liquid-nitrogen chilled, charcoal trap. Extracted gases were exposed to an SAES getter before being collected on a cryogenic cold trap at <15 K. Exclusively helium was then released by heating the cold trap to 45 K. Mass spectrometry was conducted at the LDEO Noble Gas Mass Spectrometry Laboratory using a MAP 215–50 noble gas mass spectrometer. Measurements were made relative to the Yellowstone 'Murdering Mudpot' (MM) helium standard ($^3He/^4He$ ratio of $16.45R_a$, where $R_a = {}^3He/{}^4He_{air} = 1.384 \times 10^{-6}$), using the protocol of Winckler et al. (2005).

Attenuation of cosmogenic neutron flux with depth from the surface was corrected for using measured sample thickness, a standard rock density of 2.7 g cm^{-3} and an attenuation length of 160 g cm^{-2} (Dunne et al., 1999). Field observations and inspection of satellite imagery indicate that the sampled boulders are not subject to prolonged burial by seasonal snow. Snow cover is not quantifiable for the geological past, however the topographic prominence of the boulders and moraine crests is not conducive to snow accumulation due to preferential erosion of snow by the wind. Thus, we do not apply any correction to the age calculation for burial by snow. The absence of resistant mineral veins in the local andesites precluded quantitative assessment of post-depositional erosion of boulder surfaces. Although sampled boulders did not exhibit glacial striae, some boulders retain faceted sides and care was also taken to avoid boulders that displayed clear evidence of erosion, such as discolouration, onion-skin weathering, and water pooling. We therefore choose to present the exposures ages without an erosion correction.

Regional uplift in the central North Island has been estimated at c. 0.6–1.0 mm yr^{-1} for the past 500 ka (Pulford, 2002). Integrating this uplift rate into the age calculations for boulders exposed during the LGM (c. 20–30 ka) does not alter the results outside the range of the ^3He measurement uncertainty. For the oldest samples of this study, integrating this uplift rate has the effect of increasing the exposure ages by 1–2 kyr. We present the age dataset without corrections for this effect, but discuss the implications for the glacial chronology in the text.

We present surface exposure ages calculated using the CRONUScalc MATLAB code of Marrero et al. (2015) (version 2.0) and the Lal (1991)/Stone (2000)/Nishiizumi et al. (1989) ('Lm'; Balco et al., 2008) scaling model. Recently, Lifton et al. (2014) and Borchers et al. (2015) have shown that this scaling model outperforms neutron monitor based schemes (e.g. Dunai, 2001; Desilets et al., 2006; Lifton et al., 2008). Calculation of surface exposure ages from cosmogenic ^3He concentrations requires accurate constraint of the local production rate. We take advantage of the recent, proximal calibration of cosmogenic ^3He production site situated <10 km from Mangatepopo valley (Eaves et al., 2015), which shows that the local cosmogenic ^3He production rate agrees well with global compilations of ^3He calibration datasets (e.g. Goehring et al., 2010; Borchers et al., 2015). We use the compiled production rate calibration of Borchers et al. (2015) implemented within the CRONUScalc code.

3.2. Tephrochronology

Use of discrete, isochronous, pyroclastic (primarily ash and lapilli) marker horizons as chronological tie-points in sedimentary archives of paleoenvironmental change is well established in New Zealand (e.g. Lowe et al., 2008, 2013). In glaciated landscapes, well-dated tephra layers stratigraphically overlying depositional landforms such as moraines, provide minimum ages for moraine formation, whereas tephra preserved beneath deposits of glacial outwash or till, constrains the maximum age of deposition (e.g. Kirkbride and Dugmore, 2001).

Since the work of Topping and Kohn (1973), significant progress has been made to constrain the precise age and geochemical signature of rhyolitic tephra marker horizons in New Zealand (e.g. Lowe et al., 2008, 2013; Vandergoes et al., 2013). To test the original interpretation of Topping and Kohn (1973), we revisited the soil section overlying moraine M2 in Mangatepopo valley to sample the lower two rhyolitic tephra horizons for electron microprobe (EMP) analysis of glass shard major element compositions. To aid identification, we compare the geochemistry of the sampled tephras to that of a discrete rhyolitic tephra horizon identified at Taurewa road cutting (39.12°S, 175.52°E; 825 m asl), situated c. 5 km west from the study site (Fig. 1). This tephra stratigraphically overlies the Kawakawa/Oruanui Tephra (KOT), which was recently dated at this section (c. 25.4 cal ka; Vandergoes et al., 2013).

Table 1
Location and geometry of cosmogenic^3He samples.

Sample ID	Lat. (°S)	Long. (°E)	Altitude (m asl)	Thickness (cm)	Surface strike/dip	Shielding
Moraine M1:						
MP1201	39.136	175.619	1519	2.0	0	0.998
MP1202	39.138	175.612	1429	2.0	210/10	0.998
MP1203	39.138	175.612	1429	2.0	004/4	0.998
MP1204	39.137	175.618	1481	1.5	0	0.997
MP1205	39.138	175.614	1437	2.0	312/8	0.997
Moraine M2:						
MP1206	39.141	175.598	1302	2.5	098/10	0.997
MP1207	39.141	175.600	1308	2.5	0	0.998
Moraine M3:						
MP1208	39.139	175.598	1286	2.5	0	0.998
MP1209	39.139	175.598	1280	3.0	258/6	0.998
MP1210	39.139	175.598	1275	2.5	296/2	0.998
MP1211	39.139	175.597	1266	3.0	124/2	0.998

Table 2
Helium measurement data and exposure ages for all samples. ^3He_c concentrations are derived using an assumed pyroxene crystallisation age of 110 ka (see Section 4.1). Internal uncertainty of exposure ages includes the 1σ analytical error and an assumed 20% error from the magmatic ^3He correction. Exposure ages are calculated using the scaling model of Lal (1991)/Stone (2000)/Nishiizumi et al. (1989), labelled '*Lm*' by Balco et al. (2008).

SampleID	$^3He_{total} \pm 1\sigma$ (10^6 at. g^{-1})	R/R_a	$^3He \pm 1\sigma$ (10^6 at. g^{-1})	Δ^3He (%)	Exposure age $\pm 1\sigma$ int. (Ext.) (ka)
Moraine M1:					
MP1201	11.8 ± 0.28	156	11.5 ± 0.28	−2.3	30.0 ± 0.7 (3.2)
MP1202	8.28 ± 0.17	138	8.10 ± 0.18	−2.3	23.0 ± 0.5 (2.5)
MP1203	5.64 ± 0.18	73	5.34 ± 0.19	−5.3	15.5 ± 0.5 (1.7)
MP1204	8.39 ± 0.34	172	8.27 ± 0.34	−1.4	22.5 ± 0.9 (2.5)
MP1205	9.23 ± 0.20	179	9.10 ± 0.21	−1.5	25.6 ± 0.5 (2.7)
Moraine M2:					
MP1206	6.34 ± 0.17	47	5.70 ± 0.22	−10.1	18.2 ± 0.7 (2.0)
MP1207	6.86 ± 0.19	80	6.52 ± 0.20	−5.0	20.5 ± 0.6 (2.1)
Moraine M3:					
MP1208	18.9 ± 0.33	302	18.7 ± 0.33	−1.1	57.4 ± 1.0 (6.4)
MP1209	17.4 ± 0.31	190	17.0 ± 0.32	−2.2	52.5 ± 1.0 (6.1)
MP1210	15.2 ± 0.33	195	14.9 ± 0.33	−1.9	45.9 ± 1.0 (5.1)
MP1211	16.9 ± 0.32	227	16.6 ± 0.33	−1.6	51.8 ± 1.1 (6.0)

All tephra samples were wet-sieved to isolate the >63 μm fraction, before individual glass shards were handpicked (n = >18 per sample; Table 3) and loaded in an epoxy mount. All major element determinations were made on a JEOL Superprobe (JXA-8230) at Victoria University of Wellington, using the ZAF correction method. Analyses were performed using an accelerating voltage of 15 kV under a static electron beam operating at 8 nA. The electron beam was focused to 10 μm.

3.3. Equilibrium line altitude reconstruction

Palaeoclimatic calculations from glacier reconstructions rely on accurate delineations of former ice masses, which are constrained by interpretation of ice-marginal geomorphology (Porter, 1975; Benn et al., 2005). In Mangatepopo valley, moraine ridges and glacial till extent clearly depict the terminus and lower margins of the former glacier, while erosional landforms such as glacial cirque and glacially-trimmed cliffs provide guidance on the upper glacier limits. We reconstruct the palaeo-equilibrium line altitude (*p*ELA) of the Mangatepopo glacier for the LGM only, as the older ice limits are less well preserved. In the vicinity of Mt. Ngauruhoe, post-glacial volcanic activity has obscured evidence of the former glacial limits, therefore we estimate former ice limits in this region by interpolating between the cirque headwall and the glacially-truncated lava flows of Pukekaikiore (Fig. 2). To estimate the hypsometry of the former glacier, elevation contours are drawn from the intersection of the reconstructed ice margin with the modern topographic contours. Ice surface topography is reconstructed to represent flow vectors in contemporary glaciers, which are increasingly convergent with distance upstream from the ELA, and increasingly divergent downstream (Paterson, 1994). We define the upper margins of the LGM glacier using the head of South Crater cirque (*sensu* Kaplan et al., 2010), although, it is possible that additional ice was sourced from an ice field centred on Tongariro massif (Section 2.2.2).

A number of methods exist to estimate the *p*ELA for former glaciers. The Accumulation Area Ratio (AAR) method is applied most commonly, which is based on the assumption that the accumulation zone of a steady-state glacier represents a fixed proportion of the total glacier area. Accumulation areas of modern glaciers globally, typically occupy 50–80% of the total glacier surface area (Meier and Post, 1962). Empirical studies show that New Zealand

Table 3
Glass shard major element compositions of rhyolitic tephras from the Taurewa and Mangatepopo sections, compared with potential correlatives from the Okataina Volcanic Centre (OVC). Oxide values are recalculated to 100% on a volatile-free basis. Total Fe expressed as FeOt. Mean and 1 standard deviation (*italics*), based on *n* analyses. All samples normalised either against glass standard VG-568 or ATHO-G. EMP Analyst: B.V. Alloway, for all samples except 'MP833d' (S.R. Eaves).

	SiO_2	Al_2O_3	TiO_2	FeO	MgO	MnO	CaO	Na_2O	K_2O	Cl	Total	n
Mangatepopo moraine:												
MP833(i)	78.13	12.39	0.15	0.98	0.13	0.05	0.89	3.96	3.23	0.09	98.21	20
	0.28	*0.12*	*0.03*	*0.08*	*0.01*	*0.03*	*0.04*	*0.14*	*0.10*	*0.01*	*1.28*	
MP833a(ii)	78.21	12.38	0.14	1.00	0.12	0.05	0.88	3.84	3.28	0.09	98.2	20
	0.29	*0.1*	*0.03*	*0.14*	*0.03*	*0.03*	*0.04*	*0.14*	*0.31*	*0.02*	*1.58*	
MP833d	78.86	12.39	0.14	0.91	0.13	0.05	0.88	3.5	2.99	0.15	99.3	18
	0.24	*0.10*	*0.02*	*0.09*	*0.03*	*0.03*	*0.06*	*0.14*	*0.12*	*0.02*	*1.00*	
Taurewa (SHW-47):												
Waiohau (13-16-27)	78.23	12.31	0.14	0.96	0.11	0.05	0.87	3.96	3.27	0.09	98.48	21
	0.25	*0.12*	*0.02*	*0.07*	*0.02*	*0.03*	*0.05*	*0.23*	*0.16*	*0.01*	*1.66*	
Reworked KOT? (13-16-29)	78.14	12.39	0.16	1.1	0.14	0.04	0.99	3.74	3.2	0.1	97.21	20
	0.22	*0.07*	*0.03*	*0.09*	*0.04*	*0.03*	*0.03*	*0.12*	*0.17*	*0.02*	*1.55*	
Oruanui (KOT) (13-16-30)	78.06	12.41	0.12	1.19	0.11	0.04	1.02	3.75	3.19	0.11	96.42	22
	0.19	*0.10*	*0.02*	*0.07*	*0.02*	*0.03*	*0.06*	*0.14*	*0.10*	*0.01*	*0.82*	
Standard - VG-568:												
Sept. 14 2012	75.6	12.2	0.23	3.27	0.1	0.1	1.72	3.75	2.61	nd	99.57	31
	0.55	*0.12*	*0.02*	*0.09*	*0.01*	*0.02*	*0.03*	*0.1*	*0.03*		*0.65*	
Standard - ATHO-G:												
Oct. 1 2013	75.57	12.2	0.26	3.27	0.09	0.1	1.7	3.73	2.64	0.02	99.58	48
	0.60	*0.09*	*0.03*	*0.10*	*0.01*	*0.03*	*0.03*	*0.13*	*0.05*	*0.01*	*0.75*	
Dec. 2013	75.62	12.2	0.24	3.27	0.09	0.11	1.7	3.73	2.64	0.08	99.68	20
	0.36	*0.07*	*0.02*	*0.09*	*0.01*	*0.04*	*0.02*	*0.11*	*0.06*	*0.06*	*0.41*	

glaciers most commonly have an accumulation-ablation area ratio of 2:1 (AAR = 0.67; Chinn et al., 2012).

A shortcoming of the AAR method is the failure to account for glacier hypsometry (Furbish and Andrews, 1984). Reconstructions of former valley and cirque glaciers are usually well-constrained by topography, therefore AAR-based *p*ELA estimates are subject to lower uncertainty. However, the hypsometry of former valley glaciers sourced from ice caps or plateau ice fields is less certain due to the absence of geomorphic indicators that constrain ice thickness in the upper catchment. Underestimating the planimetric surface area at the glacier head leads to underestimation of the *p*ELA, as a larger ablation area is required to balance the expanded accumulation zone. Other techniques have been developed to overcome this shortcoming in the AAR method (Furbish and Andrews, 1984; Osmaston, 2005), however these are also reliant on accurate knowledge of the former ice geometry. The glacial geomorphology of the wider Tongariro massif suggests that the former Mangatepopo glacier may have been sourced from a central ice field, as several other moraine-lined glacial valleys radiate from the centre of the edifice (Mathews, 1967), thus implying a central source. If this were the case, the AAR method will underestimate the *p*ELA, therefore we consider the AAR-based reconstructions as a maximum estimate of ELA depression from present.

Reconstructed *p*ELAs provide a useful metric for comparing the magnitude of past climate change (Porter, 1975). This requires accurate knowledge of the present-day ELA. No glaciers currently exist on Tongariro massif, however small cirque glaciers persist on Mt. Ruapehu (2797 m asl), situated 15 km to the south. In the most recent survey of these glaciers, Keys (1988) reports contemporary ELAs of 2340–2650 m asl, based on end of summer snowline surveys. Topoclimatic factors such as wind-driven snow accumulation and topographic shading impart a strong influence on the mass balance of cirque glaciers (Kuhn, 1995), which can reduce the utility of the ELA as an index for atmospheric temperature change. However, Brook et al. (2011) analysed surface area changes of one glacier on Mt. Ruapehu between AD1988–2008 and found that variations closely follow ablation season temperature changes. This correlation supports the use of end of summer snowline observations on Mt. Ruapehu to relate our *p*ELA reconstructions to past atmospheric temperature change. We take the arithmetic mean of the midpoints of Keys (1988) observations (2483 ± 55 m asl) to use as a modern (AD1988) ELA datum.

4. Results

4.1. Cosmogenic ^{3}He concentrations

Total measured ^{3}He ($^3He_{total}$) in a sample can comprise cosmogenic (^3He_c), magmatic (^3He_m), and nucleogenic (^3He_n) components. We derive ^3He_c from our measurements of $^3He_{total}$, using the following equation:

$$^3He_c = {}^3He_{total} - {}^3He_n - {}^4He_m \times (^3He/^4He)_m \quad (1)$$

^3He_n is a product of the mineral composition and crystallisation age (Andrews, 1985). Our samples exhibit low U, Th and Li concentrations, which limits ^3He_n production (Supplementary Table A1). Furthermore, the parent lavas of the moraine boulders sampled in the Mangatepopo valley are relatively young (c. 60–160 ka; Hobden et al., 1996), therefore there has been limited time for ^3He_n accumulation. The contribution of ^3He_n to $^3He_{total}$ is therefore negligible for our samples and we neglect this term from Equation (1).

^3He_m is sourced from the mantle, where $^3He/^4He$ ratios are enriched relative to the atmospheric helium ratio ($R_a = 1.384 \times 10^{-6}$). Measurements of magmatic helium in high-temperature fluids and shielded clinopyroxene phenocrysts from TgVC consistently yield $^3He/^4He$ ratios of c. $6R_a$ (Torgersen et al., 1982; Patterson et al., 1994; Hulston and Lupton, 1996), therefore we use this value for our calculations.

To calculate magmatic ^{4}He (^4He_m), we use U and Th concentrations from two samples (Supplementary Table A1) to derive the in situ production rate of radiogenic ^{4}He (^4He_r) according to Andrews (1985), and subtract this radiogenic contribution from $^4He_{total}$ ($^4He_m = {}^4He_{total} - {}^4He_r$). Neglecting ^4He_r can result in overcorrection for ^3He_m, thus causing underestimation of ^3He_c (Blard and Farley, 2008). U and Th concentrations are 0.019–0.023 ppm and 0.141–0.174 ppm, respectively (Supplementary Table A1), which yield in situ ^4He_r production rates (P_4) of $1.82–1.95 \times 10^5$ at. g^{-1} yr^{-1} (Supplementary Table A2). Given the similarity of the U and Th measurements between samples, we use the average of the two sample concentrations for samples without compositional data, which yields a ^4He_r production rate of 1.89×10^5 at. g^{-1} yr^{-1}.

To estimate ^4He_r, we use a pyroxene crystallisation age of 110 ka, which is the mid-range of the radiometric ages of Mangatepopo valley lavas dated by Hobden et al. (1996) (c. 60–160 ka). Using this age means that ^4He_r accounts for 21–59% of $^4He_{total}$ in our samples. Substituting this calculation into Equation (1) indicates that 90–99% (median = 98%) of $^3He_{total}$ in our samples is of cosmogenic origin (Table 2). Use of older crystallisation ages increases the ^4He_r component, and vice versa for younger crystallisation ages (Supplementary Table A2). Altering the crystallisation age by ±50 ka changes the ^3He_c concentrations by an average of ±0.8%, relative to the 110 ka calculation (Supplementary Table A2). Thus our ^3He_c concentrations are relatively insensitive to the choice of crystallisation age. We present exposure ages for all samples using ^3He_c reported in Table 2, which includes a 20% error for the magmatic correction propagated into the 1σ analytical uncertainty.

4.2. Cosmogenic ^{3}He results and moraine age interpretation

4.2.1. Upper moraine (M1)

Exposure ages (with internal uncertainties) of the five boulders sampled from moraine M1 are 30.0 ± 0.7 ka, 25.6 ± 0.5 ka, 23.0 ± 0.5 ka, 22.5 ± 0.9 ka and 15.5 ± 0.5 ka (Table 2). We adjudge the youngest sample (MP1203) to be an outlier, based on the preservation of moraine M2 down valley, which dates to 18–20 ka (see section 4.2.2 below). It is unlikely that M2 would be preserved today, if ice of sufficient thickness to be depositing boulder MP1203 at the elevation of M1 was present in Mangatepopo valley at c. 16 ka. Re-examination of field descriptions and photographs (e.g. Fig. 4B) suggests that this boulder may have shed a portion of its surface since deposition, as evidence of fracturing is present, probably caused by preferential weathering along internal cooling joint planes. Post-depositional removal of the boulder surface through this process provides a possible explanation for the anomalously young age.

Following omission of this geomorphic outlier, three possible depositional scenarios can explain the age distribution of the remaining four samples. First, the oldest age (c. 30 ka – MP1201) may represent inheritance of cosmogenic ^{3}He from exposure prior to deposition at its current position on the moraine crest. In this scenario, the true age of M1 would be closer to the remaining three samples, between 26 and 23 ka. Second, the oldest age (c. 30 ka – MP1201) may represent the true age of M1, with the remaining samples having been subject to post-depositional erosion of the boulder surface, or surface shielding (e.g. Ivy-Ochs et al., 2007), causing the surface exposure ages to post-date moraine formation. Third, M1 could represent a composite landform (e.g.

Roethlisberger and Schneebeli, 1979) comprising deposits from several glacier fluctuations of similar magnitude between 30 and 23 ka.

Based on the existing dataset, it is not possible to unequivocally attribute either one of these scenarios to the M1 moraine. However, analyses of large datasets of moraine boulder surface exposure ages show that only a very small percentage of boulders deposited by non-polar, temperate glaciers exhibit cosmogenic nuclide inheritance from periods of prior exposure. For example, recent dating campaigns in the Southern Alps that have generated several hundred, individual high-precision in situ cosmogenic ^{10}Be exposure ages for moraine boulders (Schaefer et al., 2009; Kaplan et al., 2010; Putnam et al., 2010a, 2013a, 2013b; Kelley et al., 2014), which indicate that any inherited component is typically less than the measurement uncertainty (see Schaefer et al., 2009 for a detailed analysis). The maritime, mid-latitude location of our study site, together with geomorphic evidence for scouring of the glacier bed (Section 2.2.1) suggest that former glaciation at this site was warm-based. Thus, while it is feasible that the ^{3}He content of MP1201 could represent inheritance from prior exposure, we consider this scenario the least likely explanation for the age distribution.

It is more difficult to decipher between the latter two scenarios, however both imply moraine aggradation at c. 30 ka, with the remaining younger ages either representing post-depositional disturbance (scenario 2), or further aggradation from glacial reoccupation at 26–23 ka (scenario 3). While scenario 2 is commonly assumed in such situations, diachronous moraines have also previously been inferred from surface exposure age datasets displaying multiple populations (e.g. Licciardi et al., 2004; Briner, 2009). This is more likely in situations where a glacier is topographically constrained (Roethlisberger and Schneebeli, 1979), such as the Mangatepopo valley. Exposure ages from down-valley (Section 4.2.2) suggest valley glaciation endured until c. 18–20 ka, therefore we suggest the age distribution from M1 most likely represents time-transgressive aggradation from persistent valley glaciation through the period c. 30–23 ka. Moraine construction would have occurred when the ice surface elevation was sufficient to overcome the prominent lava flow that bounds the northern valley side. Furthermore, we note that this interpretation is consistent with evidence from other glaciated catchments in New Zealand, which indicate glacier termini were at or near their maximum downstream limits for the last glacial cycle between c. 30–18 ka (e.g. Putnam et al., 2013b; Kelley et al., 2014; Rother et al., 2014; see Discussion).

4.2.2. Lower moraine – inner (M2)

Two boulders were deemed suitable for exposure dating (MP1206 and MP1207; Fig. 4C and D) and returned ages of 18.2 ± 0.7 ka and 20.5 ± 0.6 ka, respectively. These ages are in close agreement and are stratigraphically coherent with the age of M1 and the overlying tephrostratigraphy (Section 4.3).

4.2.3. Lower moraine – outer (M3)

Samples were collected from four boulders, which returned ages ranging from 57.4 ± 1.0 ka to 45.9 ± 1.0 ka. We consider these ages to be minimum-limiting ages for this landform for the following reasons.

Continual exposure of these andesitic boulders to the relatively high total annual precipitation at this location (c. 3 m yr^{-1}; NIWA, 2014), over several tens of millennia, is likely to have caused granular disintegration of the boulder surfaces. Such erosion would remove cosmogenic ^{3}He atoms, thus resulting in nuclide concentrations that underestimate the true exposure age of the boulder. For example, if the sampled boulders on moraine M3 have been exposed since c. 63 ka, which corresponds with the culmination of a major glacier advance in the Southern Alps (Schaefer et al., 2015), then surface erosion rates of 1.5–5.5 mm kyr^{-1} are required to replicate our observed exposure ages. Such rates of rock erosion agree well the compilation of Portenga and Bierman (2011) which indicates typical long term erosion rates of 1–10 mm kyr^{-1} for igneous lithologies in temperate climatic environments.

Our age calculations are uncorrected for potential tectonic uplift during the period of exposure, which has been estimated at c. 0.6–1.0 mm yr^{-1} (Pulford, 2002). Including c. 40–60 m of uplift into the exposure age calculation serves to lower the time-integrated local production rate relative to that estimated for the present day sample elevation. Depending on the temporal pattern of uplift over the exposure period, this effect could contribute to underestimation of boulder ages by up to 2 kyr.

All boulders on the moraine have been subject to similar tectonic uplift, thus this effect should be uniform between samples. The effects of boulder surface erosion is likely to have impacted individual boulders to varying degrees (e.g. due to differences in rock hardness), thus contributing to the scatter amongst the exposure ages. We therefore consider that the oldest samples, which yield exposure dates of 52–57 ka, represent the closest minimum age constraint for the true age of moraine M3. However the true moraine age may be several millenia older still (see Discussion).

4.3. Coverbed stratigraphy and tephra major element geochemistry

Stratigraphic logging of soil sections overlying the ice-proximal flank of the M2 moraine (Fig. 5A) permits correlation with the detailed descriptions of Topping and Kohn (1973) and Topping (1974). At c. 450 cm depth we identify a matrix-supported diamicton, predominantly consisting of boulders and cobbles in a silty matrix, which represents the surface of the underlying lateral moraine. A section containing approximately 90 cm of interbedded cm-to dm-thick andesitic ash and lapilli beds, with two yellow-white rhyolitic tephra beds and weakly formed palaeosols, immediately overlies the moraine surface. The lowermost rhyolitic tephra (sample: 'MP833a') is 0.2–1 cm thick and situated c. 10–20 cm above the moraine surface, immediately overlying a 3 cm thick, coarse (med. sand), dark-grey andesitic tephra (Fig. 5C). The lower rhyolitic tephra exhibits ductile fold structures (Fig. 5B), which suggests post-depositional deformation, perhaps via frost-heave. Approximately 40 cm above MP833a, a discontinuous rhyolitic tephra (sample: 'MP833d') varies in thickness from 0 to 3 cm (Fig. 5C). We identify a distinct cobble-to-fine gravel unit at 350 cm depth, which we correlate to the pebble unit identified by Topping and Kohn (1973) (described fully in Topping, 1974), therefore we are confident that these tephra samples correspond with those analysed by Topping and Kohn (1973). A sharp erosional contact separates this coarse unit from a massive, grey/brown silt–clay bed (300–50 cm depth), with abundant rhizomorphs and two, discrete, interbedded pumiceous horizons. The lower pumice bed (at c. 275 cm depth) is c. 10 cm thick and consists of yellow and dark brown coloured clasts, up to 2 cm in diameter. The upper pumice is c. 40–50 cm thick and immediately underlies the modern soil horizon. This pumice is correlated to the Taupo ignimbrite (AD232 ± 10 yr; Lowe et al., 2013), based on stratigraphic position, large pumice clasts (up to 10 cm diameter), and abundant charred twigs.

Shane (2000) summarised the major element chemistry of post-25 ka rhyolitic tephras in North Island and found that OVC tephras are characterised by higher SiO_2 (c. 76–79 wt. %) and lower FeO (c. 1 wt. %), compared to those from the Taupo Volcanic Centre (SiO_2 = c. 71–77 wt. %; FeO = 1.5–3.5 wt. %). Using this information, we can assign samples MP833a and MP833d (Table 3; Fig. 6) to the

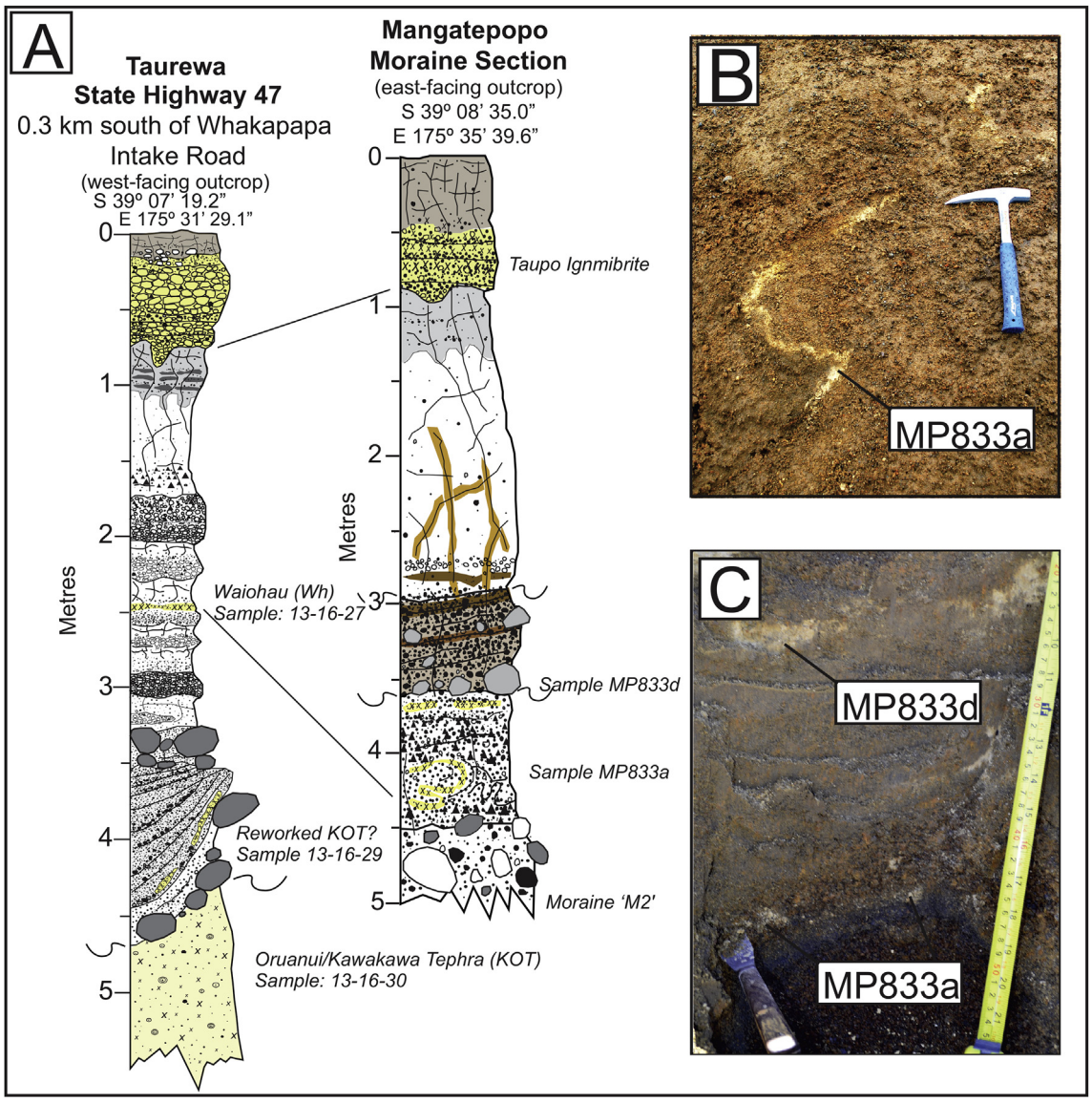

Fig. 5. (A) Stratigraphic log of the Taurewa reference section and the Mangatepopo moraine section originally described by Topping and Kohn (1973), with the samples labelled; (B) The lowermost rhyolitic tephra (sample MP833a) exhibiting deformation structures likely caused by gelifluction in a formerly frozen soil (Photo: B.V. Alloway); (C) Soil pit showing both rhyolite horizons at the Mangatepopo section.

OVC with high confidence. This supports the original interpretation of Topping and Kohn (1973), who assigned both to horizons in the Mangatepopo section to OVC-sourced eruptions. However, the major element compositions of MP833a and MP833d are also indistinguishable from one another (Table 3; Fig. 6), which suggests that the upper sample (MP833d) could represent a reworked remnant of MP833a below. This inference is further supported by the field observations of deformation structures within the lower horizon (MP833a), but contradicts the initial interpretation of Topping and Kohn (1973). The geochemical composition of the Taurewa rhyolitic tephra (Sample: 13-16-27; Fig. 5) is indistinguishable from the Mangatepopo data, which suggests that it represents the same volcanic event (Fig. 6).

To further constrain deglaciation in the Mangatepopo valley, we seek to determine which OVC-sourced event is represented by the Mangatepopo tephra. To do this, we compare the glass shard major element measurements to proximal and distal OVC reference data from Honeycomb Trench (B.V. Alloway, *unpub. data*) and Waipaoa river basin (Bilderback, 2012; Marden et al., 2014), respectively. The Mangatepopo and Taurewa data are sufficiently different from the Rotorua Tephra for us to rule this out as a possible correlative (Fig. 6). Using binary plots of K_2O–FeO, the Rerewhakaaitu Tephra can be readily discriminated from the Waiohau Tephra by the presence of high and low K_2O populations in the former (Fig. 6B; Shane et al., 2008). The Mangatepopo samples display a single K_2O population, which is consistent with the Waiohau Tephra in the proximal reference datasets (Fig. 6). Furthermore, biotite has been noted as a diagnostic component of the ferromagnesian mineral assemblage of the Rerewhakaaitu Tephra (Froggatt and Lowe, 1990) and we do not identify any biotite flakes within the mineral assemblages of the samples. Isopach maps of tephra dispersal over North Island (Lowe et al., 2013) indicate a similar thickness (0.5–1 cm) for both the Rerewhakaaitu and Waiohau tephras in the vicinity of the study site, therefore field observations of thickness are not useful in discriminating between the two.

In summary, field descriptions and EMP measurements of glass

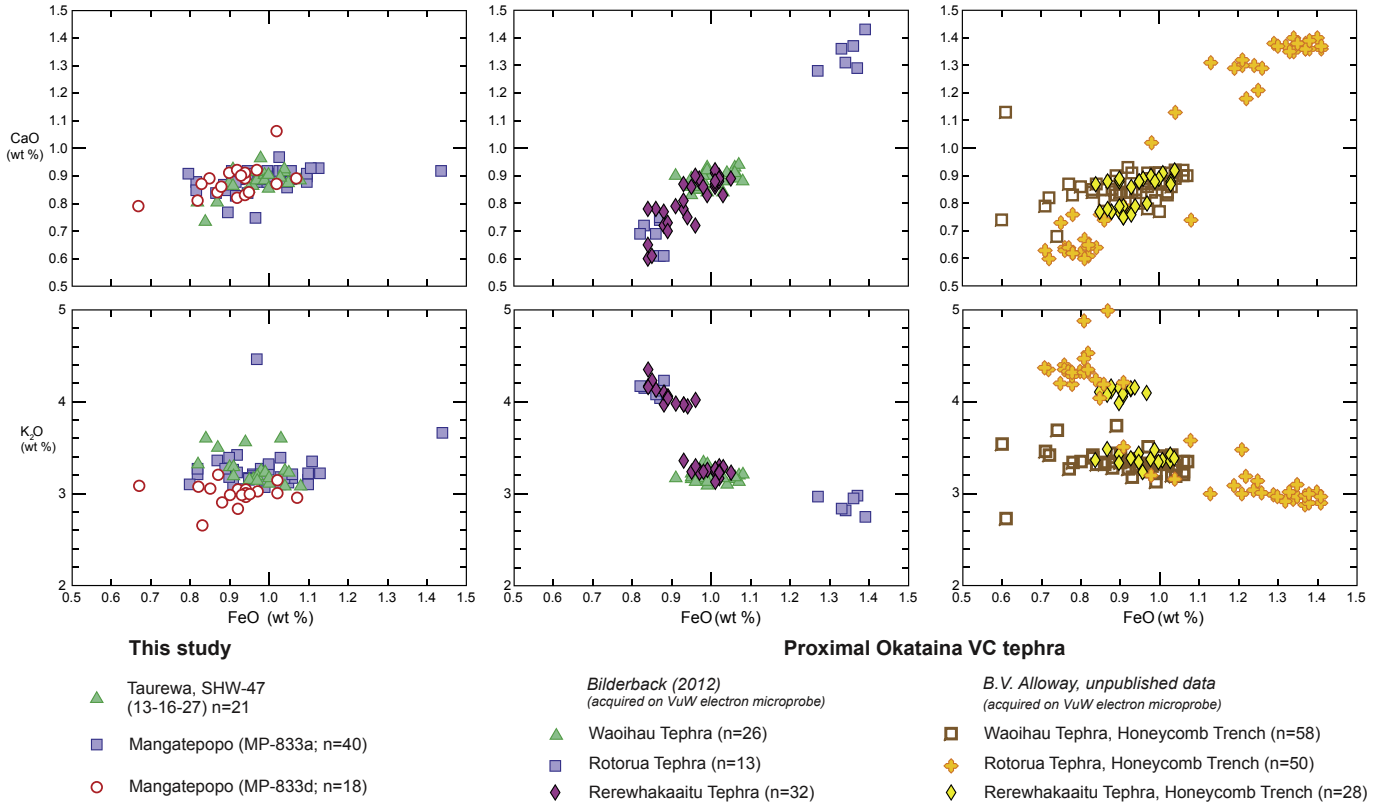

Fig. 6. Glass shard FeO vs. K_2O and CaO (wt. %) plots of Mangatepopo samples compared with OVC-proximal (Honeycomb Trench) and north-eastern North Island distal (Waipaoa) reference data. All major element EMP glass data was acquired on the same analytical instrument at Victoria University of Wellington under the same operational conditions and using the same internal standards.

shard major elements suggest that the samples from two rhyolitic tephra horizons likely represent the same event, as opposed to the previous interpretation of two separate events (Topping and Kohn, 1973). Furthermore, the major element composition of this tephra can be correlated to the OVC with high confidence. The body of field-evidence, mineralogy and glass geochemistry all strongly indicate that the ash layer is likely to be Waiohau Tephra, which was emplaced at c. 14.0 ± 0.2 cal ka BP (Lowe et al., 2013). This result is stratigraphically consistent with surface exposure ages from the moraine crest (c. 18–20 ka; Section 4.2.2) and accords with moraine-tephrostratigraphy elsewhere on Tongariro massif (Cronin and Neall, 1997) that suggests moraine abandonment and soil aggradation was well underway prior to c. 14 ka, in response to climatic amelioration. This represents a minimum age for ice-retreat, which likely occurred several thousands of years earlier, as indicated by the cosmogenic surface exposure ages on the moraine crest.

4.4. Equilibrium line altitude reconstruction

We derive a *p*ELA (AAR = 0.67; Chinn et al., 2012) for the LGM Mangatepopo glacier of c. 1410 m asl (Fig. 7a). This is in reasonable agreement with the maximum elevation of lateral moraine (MELM; Andrews, 1975) M1 at c. 1530 m asl, which can be used to approximate the *p*ELA associated with the older (c. 30–23 ka), slightly thicker Mangatepopo glacier. The moraine stratigraphy suggests that the Mangatepopo glacier was broadly of similar extent during the period 30–18 ka, therefore the MELM method provides a useful independent test of the AAR-based ELA estimate, particularly as it is not subject to uncertainties in past glacier hypsometry or topographic change. Preservation of the slightly older moraine M1 implies the *p*ELA associated with M2 cannot be lower than 1530 m asl. The lower value returned by the AAR method is thus likely to reflect minor uncertainties in the palaeoglacier reconstruction either caused by post-glacial topographic change, and/or the former presence of a wider accumulation zone than currently appreciated, such as an ice field (e.g. Rea et al., 1999). Given the uncertainties in both methods of *p*ELA reconstruction, we consider 1400–1550 m asl a most-likely estimate of the ELA in Mangatepopo valley during the period 30–18 ka. This represents an ELA lowering of c. 930–1080 m, relative to the contemporary ELA datum of Keys (1988) (2483 ± 55 m asl).

The ELA on a given glacier is primarily controlled by summer air temperature and winter precipitation, although a range of other energy-balance (insolation, local wind speed, cloudiness, humidity) and topoclimatic (avalanching, snow drifting, topographic shading) factors also contribute (Oerlemans and Fortuin, 1992). Assuming no change in precipitation, it is possible to derive a first-order estimate of atmospheric temperature change associated with a *p*ELA reconstruction, using a temperature lapse rate. Temperature lapse rates can vary significantly in space and time (Doughty et al., 2013), and ELA-based palaeotemperature reconstructions are sensitive to this value. For example, we calculate an LGM temperature lowering of c. 5.4 °C relative to present, when using the mean annual temperature lapse rate for upland (>300 m) New Zealand (−5.1 °C km^{-1}; Norton, 1985). However, using the standard environmental lapse rate (−6.5 °C km^{-1}) increases the temperature depression estimate to 7.0 °C. Fig. 7b shows the cumulative probability distribution of palaeotemperature estimates in Mangatepopo valley derived using the empirically constrained palaeo- (1400–1550 m asl; AAR and MELM) and contemporary (2483 ± 55 m asl; Keys, 1988) ELAs, and a range of possible atmospheric temperature

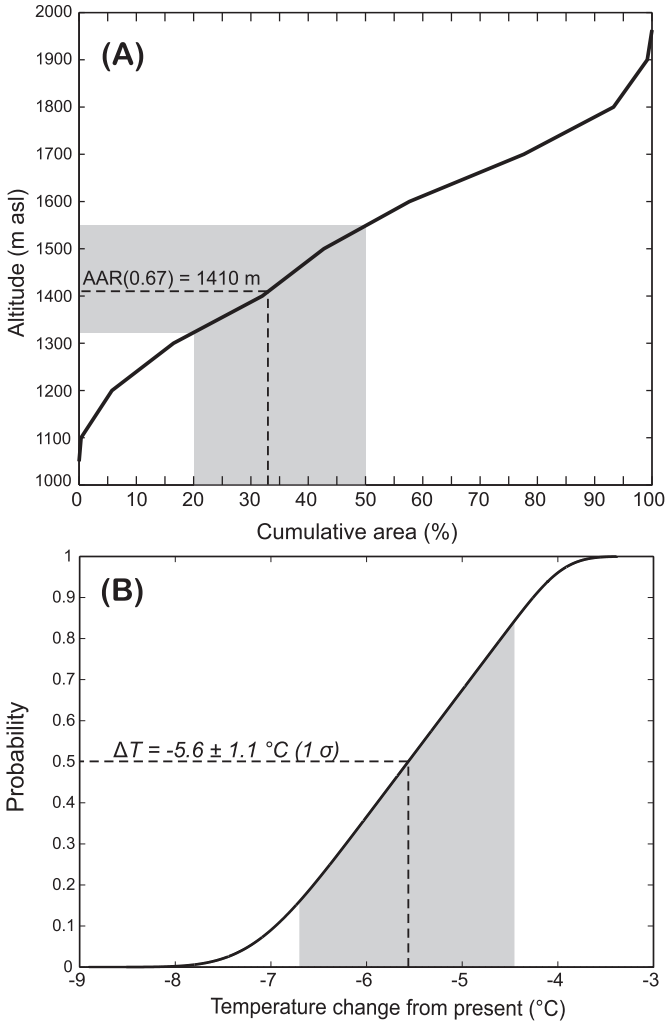

Fig. 7. (a) Area-altitude curve for the reconstructed LGM Mangatepopo glacier. Solid line depicts the associated ELA derived using an AAR of 0.67. Grey shading indicates range using the AAR values of 0.5–0.8 (Meier and Post, 1962). (b) Cumulative probability distribution function of the palaeotemperature estimate in the Mangatepopo valley derived using palaeo- (1400–1550 m asl; AAR and MELM) and contemporary-ELAs (2483 ± 55 m asl; Keys, 1988) and a range of possible atmospheric temperature lapse rates, equally weighted between 4 and 7 °C km^{-1}. Shaded grey zone indicates 1σ uncertainty interval.

lapse rates, equally weighted between 4 and 7 °C km^{-1}. This yields a normally distributed range of palaeotemperature estimates, centred on 5.6 ± 1.1 °C (Fig. 7a), which we consider to be a best-estimate estimate of temperature anomaly in central North Island between 30 and 18 ka.

5. Discussion

5.1. The Last Glacial Maximum in central North Island

Using cosmogenic ^{3}He surface exposure dating of moraine boulders, we provide the first direct chronological constraint for extensive valley glaciation on Tongariro massif during MIS 3–2, which began as early as 30 ± 3 ka and persisted until at least c. 18–20 ka. This is well-aligned, within dating errors, with the Last Glacial Cold Period (LGCP; c. 29–18 ka) as identified in the New Zealand Climate Event Stratigraphy (Barrell et al., 2013). The local ELA depression associated with LGCP glaciation in Mangatepopo valley was c. 1400–1550 m asl (Fig. 7). The timing and magnitude of these changes are in good agreement with previous palaeoenvironmental reconstructions from central North Island. On Mt. Ruapehu, situated c. 15 km to the south of Mangatepopo valley, McArthur and Shepherd (1990) report geomorphological evidence for a former ice mass with an equilibrium line of 1500–1600 m asl, which agrees well with our proximal *p*ELA reconstruction. McArthur and Shepherd (1990) suggest deformed pro-glacial lake sediments interbedded with moraines on northeast Ruapehu record multiple glacier advances during the last glacial cycle. Topping (1974) identified the Kawakawa-Oruanui Tephra within these lake sediments, which places glacier advances either side of 25.4 ka. The latter advance likely correlates to the final stand of the Mangatepopo glacier at 18–20 ka, however the lack of direct dating on Mt. Ruapehu means the timing of preceding glacier fluctuations is unconstrained.

Our new glacial chronology for central North Island exhibits good agreement with the only other LGM glacial reconstruction in North Island, New Zealand. Brook et al. (2008) report cosmogenic ^{10}Be moraine and bedrock exposure ages of c. 18 ka in Park Valley of the Tararua ranges of southern North Island (c. 40°S). Recalculating these ages using the local ^{10}Be production rate of Putnam et al. (2010b) yields revised ages of c. 19–21 ka, which is indistinguishable from the M2 moraine in the Mangatepopo valley. Brook (2009) also identifies the KOT within the Park Valley moraine, which suggests it represents a composite feature first occupied prior to 25.4 ka (Brook and Crow, 2008; Brook, 2009). This evidence is also in agreement with our findings that the M1 and M2 moraines were constructed between 30 and 18 ka.

Recent, high-precision cosmogenic ^{10}Be moraine chronologies from the central Southern Alps show a similar temporal pattern of glacier fluctuations. Local constraint of the ^{10}Be production rate (Putnam et al., 2010b), coupled with favourable topographic situations for moraine preservation and extensive exposure age datasets, have afforded detailed insight to late Quaternary glacier fluctuations in this region. For example, Putnam et al. (2013b) show that the former Ohau glacier deposited terminal moraines at c. 32 ka, c. 27 ka c. 23 ka and c. 18 ka. Similarly, the nearby Pukaki glacier attained its maximum LGCP length by 28 ka and fluctuated about this position until 18 ka (Schaefer et al., 2006; Kelley et al., 2014; Schaefer et al., 2015). On the west coast of South Island, Suggate and Almond (2005) suggest glacier advances culminated at c. 28 ka, 22 ka and 19 ka, however recent cosmogenic ^{10}Be surface exposure dating of these moraine sequences has refined the age of these deposits to c. 25 ka, c. 21 ka and c. 17 ka (Barrows et al., 2013). On the eastern side of the Southern Alps, Rother et al. (2014) show that the former Rangitata glacier reached its maximum extent before c. 28 ka, followed by successive fluctuations of slightly lesser extent between 26 and 19 ka. In the south, Williams et al. (2015) report that speleothem growth in Aurora Cave ceased at c. 33 ka when a glacier advanced in the Te Anau trough. Thus, our findings from central North Island add to a growing body of evidence that show glaciers across New Zealand attained their maximum extent in late MIS 3 and fluctuated about this position through the global LGM (26–19 ka; Clark et al., 2009).

At the last glacial termination, the Mangatepopo glacier persisted until 18–20 ka, as indicated by the cosmogenic ^{3}He moraine chronology. Additional constraint from moraine tephrostratigraphy in the Mangatepopo valley, suggests significant climatic amelioration and glacier retreat occurred prior to deposition of the Waiohau Tephra (c. 14.0 ± 0.2 ka; Lowe et al., 2013). Several catchments in the Southern Alps exhibit evidence for moraine formation at c. 20–22 ka and c. 18 ka (Schaefer et al., 2006; Putnam et al., 2013b; Kelley et al., 2014). It is possible that a similar moraine sequence is preserved in the Mangatepopo valley, but remains undated. For example, we note that multiple, sharp-crested moraines exist on

the southern side of Mangatepopo valley (Fig. 2). However, thick overlying soil sequences at these lower altitudes preclude exposure dating of these moraines.

The palaeoglacier reconstruction for Mangatepopo valley indicates local atmospheric temperature was reduced by 5.6 ± 1.1 °C relative to present (Fig. 7b) during the LGM. This estimate assumes that precipitation during the LGM was similar to present. Currently there is a paucity of quantitative LGM precipitation estimates in New Zealand, however proxy-, glacier model-, and climate model-based reconstructions are generally consistent in suggesting that annual precipitation was similar or slightly reduced, relative to present (Drost et al., 2007; Rojas et al., 2009; Whittaker et al., 2011; Golledge et al., 2012; Lorrey et al., 2012; Stephens et al., 2012). Reduced annual precipitation in central North Island during the LGM would increase the magnitude of atmospheric cooling required to explain the reconstructed ELA. However, empirical and glacier model-based evidence suggests that past and present-day glacier mass balance in New Zealand is relatively insensitive to precipitation change, with precipitation increases of c. 30–80% required to balance 1 °C of warming (Oerlemans, 1997; Anderson and Mackintosh, 2006, 2012; Anderson et al., 2010). Thus, the error in the palaeotemperature estimate arising from past precipitation change is relatively insignificant (<1 °C) in comparison to the uncertainty in the ELA reconstruction and temperature lapse rate.

Our LGM temperature estimate for central North Island exhibits good agreement with catchment- and regional-scale glacier model simulations of LGM glaciers in the Southern Alps, which indicate temperature depression of c. 6–7 °C relative to present (Golledge et al., 2012; McKinnon et al., 2012; Putnam et al., 2013b; Rowan et al., 2013). The estimate also agrees with quantitative LGM temperature reconstructions from dissolved noble gases in groundwater (3.7–6.2 °C; Seltzer et al., 2015) and fossil pollen assemblages (6.0 ± 1.9 °C – Newnham et al., 2013). Offshore, estimates of local sea surface palaeotemperatures vary spatially, but also tend to converge on a 4–7 °C lowering between c. 30–18 ka (Pahnke and Sachs, 2006; Barrows et al., 2007; Bostock et al., 2013).

5.2. Pre-LGM glaciation

Cosmogenic ^{3}He surface exposure ages from moraine M3 in Mangatepopo valley indicate that the former Mangatepopo glacier attained its maximum extent of the last glacial cycle prior to the LGM. Surface erosion and tectonic uplift of the samples from the M3 moraine, which have been exposed since at least c. 57 ka, means that the exposure ages are likely to represent minimum ages for moraine formation. Thus, the true moraine age is probably older, perhaps by several millenia. Although undated, the moraine sequences in the nearby Makahikatoa Stream catchment (Fig. 2) exhibit similar morphology and morphostratigraphic relationships to those in Mangatepopo valley, which further supports our interpretation of a widespread glacier advance on Tongariro massif, which occurred prior to the LGM. Below, we consider this interpretation in the context of other geological records of glacial fluctuations during this time period.

Elsewhere in New Zealand, evidence for pre-LGM glacial expansion during the last glacial cycle remains relatively scarce. Where present, the timing is often poorly constrained. However, a recent high-precision cosmogenic ^{10}Be exposure age dataset from the Balmoral moraines in central Southern Alps shows that an advance of the former Pukaki and Tekapo glaciers culminated at 65 ± 3 ka (n = 39, plus three outliers; Schaefer et al., 2015). The Balmoral moraines associated with this advance (Barrell, 2014) are present outboard of the well-dated, local LGM limits (Schaefer et al., 2006; Kelley et al., 2014; Schaefer et al., 2015), thus indicating that the glaciers attained their maximum extent of the last glacial cycle prior to the LGM. Sutherland et al. (2007) present cosmogenic ^{10}Be surface exposure ages from a suite of moraines preserved on Cascade plateau (44°S), on the west coast of South Island. The moraine belt immediately outboard of the LGM limits at this location yielded boulder exposure ages of c. 60–68 ka (n = 2, plus one outlier) when recalculated according to Putnam et al. (2010b). These revised ages provide further evidence for a glacial advance during MIS 4, which was of similar magnitude to the LGM.

Other glacial records from South Island also indicate glacier expansion around this time, however the chronologies are less-precisely constrained, largely relying on bracketing luminescence ages from ice-marginal deposits. For example, McCarthy et al. (2008) present evidence from the Tasman Mountains in northern South Island (41 °S) that suggests two periods of glaciation, of similar magnitude, occurred during MIS 4 and the LGM. The MIS 4 glaciation at this location is constrained with optically-stimulated luminescence ages of glacio-lacustrine deposits, which are present outboard of the LGM limits, and date to 64 ± 10 ka. On the central west coast of South Island, luminescence ages of sand/silt beds interbedded with glacial outwash gravels suggest glacier expansion at c. 85 ka and c. 64 ka (Preusser et al., 2005). However, moraines correlated with these outwash deposits have recently been shown to date to c. 25 ka (Barrows et al., 2013). No moraines of MIS 4 age were recognised by Barrows et al. (2013), therefore they suggest that any such deposits were overrun during the LGM when glaciers in this catchment attained their maximum extent of the last glacial cycle.

There is little evidence for any significant glacier advances in New Zealand between 60 and 45 ka (Williams et al., 2015), during which period fall most of the exposure ages from M3 moraine, if taken at face value. Furthermore, continuous climate proxy data indicate that this time period was characterised by relatively mild, interstadial conditions (Shulmeister et al., 2001; Shane and Sandiford, 2003; Whittaker et al., 2011; Williams et al., 2015), which were probably unfavourable for significant glacier advance. Offshore, Barrows et al. (2007) identify intervals of high clastic sediment input between 70 and 60 ka in multiple cores, which are intepreted to represent higher terrestrial erosion rates due to expansion of nearby mountain glaciers. This is followed by a sharp reduction after 60 ka, which is consistent with the terrestrial evidence for climatic amelioration and glacial retreat. Thus, the majority of evidence from glacial records and other climate proxies support our interpretation that the M3 moraine is likely to represent glacier advance in central North Island during late MIS 4 (c. 65–60 ka).

6. Conclusions

1. Tongariro massif was last glaciated between 30 and 18 ka when a central ice field fed valley glaciers that extended down to c. 1200 m asl. The onset of glacial retreat occurred c. 18–20 ka, which is in agreement with the only other moraine ages in North Island (Brook et al., 2008). The timing of glaciation in central North Island is also consistent with a growing body of evidence that shows mountain glaciers in Southern Alps attained their maximum Last Glacial Maximum extents by 32–28 ka and persisted until the onset of the last glacial termination (Schaefer et al., 2006; Putnam et al., 2013b; Kelley et al., 2014; Rother et al., 2014; Schaefer et al., 2015).
2. During the Last Glacial Maximum, the local equilibrium line altitude in central North Island was c. 1400–1550 m asl, which is 930–1080 m lower than present. This equates to a best-estimate temperature depression of 5.6 ± 1.1 °C, when uncertainties in the ELA reconstruction and temperature lapse rate are considered. This is good agreement with palaeotemperature estimates from

glacier modelling (Golledge et al., 2012; McKinnon et al., 2012; Putnam et al., 2013b) and other climate proxy reconstructions (Newnham et al., 2013; Seltzer et al., 2015).

3. Reinvestigation of the moraine coverbed stratigraphy, using field observations and major element analysis, indicates that the rhyolitic tephra close to the moraine surface is the Waiohau Tephra. This presence of this well-dated tephra within a palaeosol overlying the innermost moraine indicates that climatic amelioration following the LGM was well advanced in central North Island by c. 14 cal. ka BP.
4. Cosmogenic ^{3}He surface exposure ages from boulders on the outermost lateral moraine identified in the Mangatepopo valley indicate that glaciers on Tongariro massif attained their greatest extent of the last glacial cycle prior to the global Last Glacial Maximum. Geological processes such as boulder surface erosion and tectonic uplift mean that these ages provide minimum limiting constraint of the moraine age and the true age is likely older by several millennia. This evidence, together with comparison to glacier records from Southern Alps (e.g. Schaefer et al., 2015) and other continuous climate proxy data (e.g. Barrows et al., 2007; Williams et al., 2015), indicates that this glacial advance most likely occurred late in Marine Isotope Stage 4 (c. 65–60 ka).

Acknowledgements

S.R.E. was supported by the Victoria University Doctoral Scholarship, a VUW Faculty Strategic Research Grant and the Antarctic Research Centre Endowed Development Fund. J.M.S. and G.W. acknowledge support by the Lamont Climate Center and the Comer Science and Educational Foundation as well as by the NSF-EAR award No. 0823521. Jenni Hopkins and Richard Jones assisted with fieldwork. Roseanne Schwartz, Linda Baker and Sascha Serno provided invaluable assistance with sample preparation and mass spectrometry. We also thank Fred Luiszer (University of Colorado) for major and trace element analyses. Permission for sample collection was granted by Dept. of Conservation contract DM-593774. This is LDEO contribution number 7947.

Appendix A. Supplementary data

Supplementary data related to this article can be found at http://dx.doi.org/10.1016/j.quascirev.2015.11.004.

References

Almond, P., Moar, N., Lian, O., 2001. Reinterpretation of the glacial chronology of South Westland, New Zealand. N. Z. J. Geol. Geophys. 44, 1–15.
Anderson, B., Mackintosh, A., 2006. Temperature change is the major driver of late-glacial and Holocene glacier fluctuations in New Zealand. Geology 34, 121–124.
Anderson, B., Mackintosh, A., 2012. Controls on mass balance sensitivity of maritime glaciers in the Southern Alps, New Zealand: the role of debris cover. J. Geophys. Res. Earth Surf. 117, F01003.
Anderson, B., Mackintosh, A., Stumm, D., George, L., Kerr, T., Winter Billington, A., Fitzsimons, S., 2010. Climate sensitivity of a high-precipitation glacier in New Zealand. J. Glaciol. 56, 114–128.
Andrews, J., 1975. Glacial Systems. An Approach to Glaciers and their Environments. Duxbury Press, North Scituate, USA.
Andrews, J., 1985. The isotopic composition of radiogenic helium and its use to study groundwater movement in confined aquifers. Chem. Geol. 49, 339–351.
Balco, G., Stone, J.O., Lifton, N.A., Dunai, T.J., 2008. A complete and easily accessible means of calculating surface exposure ages or erosion rates from ^{10}Be and ^{26}Al measurements. Quat. Geochronol. 4, 93–107.
Barrell, D.J.A., 2014. The Balmoral moraines near Lake Pukaki, Southern Alps: a new reference area for the early Otira Glaciation in New Zealand. N. Z. J. Geol. Geophys. 57, 442–452.
Barrell, D.J.A., Almond, P.C., Vandergoes, M.J., Lowe, D.J., Newnham, R.M., 2013. A composite pollen-based stratotype for inter-regional evaluation of climatic events in New Zealand over the past 30,000 years (NZ-INTIMATE project). Quat. Sci. Rev. 74, 4–20.
Barrows, T.T., Almond, P., Rose, R., Keith Fifield, L., Mills, S.C., Tims, S.G., 2013. Late Pleistocene glacial stratigraphy of the Kumara-Moana region, West Coast of South Island, New Zealand. Quat. Sci. Rev. 74, 139–159.
Barrows, T.T., Juggins, S., De Deckker, P., Calvo, E., Pelejero, C., 2007. Long-term sea surface temperature and climate change in the Australian-New Zealand region. Paleoceanography 22, PA2215.
Benn, D.I., Owen, L.A., Osmaston, H.A., Seltzer, G.O., Porter, S.C., Mark, B., 2005. Reconstruction of equilibrium-line altitudes for tropical and sub-tropical glaciers. Quat. Int. 138–139, 8–21.
Bilderback, E.L., 2012. Hillslope Response to Climate-modulated River Incision and the Role of Deep-seated Landslides in Post-glacial Sediment Flux: Waipaoa Sedimentary System, New Zealand. Ph.D. Thesis. University of Canterbury, New Zealand.
Blard, P.H., Farley, K.A., 2008. The influence of radiogenic 4He on cosmogenic ^{3}He determinations in volcanic olivine and pyroxene. Earth Planet. Sci. Lett. 276, 20–29.
Borchers, B., Marrero, S., Balco, G., Caffee, M., Goehring, B., Lifton, N., Nishiizumi, K., Phillips, F., Schaefer, J., Stone, J., 2015. Geological calibration of spallation production rates in the cronus-earth project. Quat. Geochronol. http://dx.doi.org/10.1016/j.quageo.2015.09.005.
Bostock, H., Barrows, T., Carter, L., Chase, Z., Cortese, G., Dunbar, G., Ellwood, M., Hayward, B., Howard, W., Neil, H., Noble, T., Mackintosh, A., Moss, P., Moy, A., White, D., Williams, M., Armand, L., 2013. A review of the AustralianNew Zealand sector of the Southern Ocean over the last 30 ka (Aus-INTIMATE project). Quat. Sci. Rev. 74, 35–57.
Briner, J.P., 2009. Moraine pebbles and boulders yield indistinguishable ^{10}Be ages: a case study from Colorado, USA. Quat. Geochronol. 4, 299–305.
Bromley, G.R., Winckler, G., Schaefer, J.M., Kaplan, M.R., Licht, K.J., Hall, B.L., 2014. Pyroxene separation by HF leaching and its impact on helium surface-exposure dating. Quat. Geochronol. 23, 1–8.
Brook, M.S., 2009. Lateral moraine age in Park Valley, Tararua Range, New Zealand. J. R. Soc. N. Z. 39, 63–69.
Brook, M.S., Crow, T.V.H., 2008. A debris ridge in Park Valley, Tararua Range, New Zealand as evidence for Pleistocene glaciation. N. Z. J. Geol. Geophys. 51, 23–28.
Brook, M.S., Dean, J.F., Keys, H.J.R., 2011. Response of a mid-latitude cirque glacier to climate over the last two decades: Mangaehuehu Glacier, Mt Ruapehu. Earth Surf. Process. Landf. 36, 1973–1980.
Brook, M.S., Shulmeister, J., Crow, T.V.H., Zondervan, A., 2008. First cosmogenic ^{10} Be constraints on LGM glaciation on New Zealand's North Islands: Park Valley, Tararua Range. J. Quat. Sci. 23, 707–712.
Chinn, T., Fitzharris, B.B., Willsman, A., Salinger, M.J., 2012. Annual ice volume changes 1976–2008 for the New Zealand Southern Alps. Glob. Planet. Change 92–93, 105–118.
Clark, P.U., Dyke, A.S., Shakun, J.D., Carlson, A.E., Clark, J., Wohlfarth, B., Mitrovica, J.X., Hostetler, S.W., McCabe, A.M., 2009. The Last Glacial Maximum. Science 325, 710–714.
Columbus, J., Sirguey, P., Tenzer, R., 2011. A free, fully accessible 15-m DEM for New Zealand. Surv. Q. 66, 16–19.
Cronin, S.J., Neall, V.E., 1997. A late quaternary stratigraphic framework for the northeastern Ruapehu and eastern Tongariro ring plains, New Zealand. N. Z. J. Geol. Geophys. 40, 185–197.
Denton, G.H., Anderson, R.F., Toggweiler, J.R., Edwards, R.L., Schaefer, J.M., Putnam, A.E., 2010. The last glacial termination. Science 328, 1652–1656.
Desilets, D., Zreda, M., Prabu, T., 2006. Extended scaling factors for in situ cosmogenic nuclides: new measurements at low latitude. Earth Planet. Sci. Lett. 246, 265–276.
Donoghue, S.L., Neall, V.E., Palmer, A.S., 1995. Stratigraphy and chronology of late Quaternary andesitic tephra deposits, Tongariro volcanic Centre, New Zealand. J. R. Soc. N. Z. 25, 115–206.
Doughty, A.M., Anderson, B.M., Mackintosh, A.N., Kaplan, M.R., Vandergoes, M.J., Barrell, D.J.A., Denton, G.H., Schaefer, J.M., Chinn, T.J.H., Putnam, A.E., 2013. Evaluation of Lateglacial temperatures in the Southern Alps of New Zealand based on glacier modelling at Irishman Stream, Ben Ohau Range. Quat. Sci. Rev. 74, 160–169.
Drost, F., Renwick, J., Bhaskaran, B., Oliver, H., McGregor, J., 2007. A simulation of New Zealand's climate during the Last Glacial Maximum. Quat. Sci. Rev. 26, 2505–2525.
Dunai, T.J., 2001. Influence of secular variation of the geomagnetic field on production rates of in situ produced cosmogenic nuclides. Earth Planet. Sci. Lett. 193, 197–212.
Dunne, J., Elmore, D., Muzikar, P., 1999. Scaling factors for the rates of production of cosmogenic nuclides for geometric shielding and attenuation at depth on sloped surfaces. Geomorphology 27, 3–11.
Eaves, S.R., Winckler, G., Schaefer, J.M., Vandergoes, M.J., Alloway, B.V., Mackintosh, A.N., Townsend, D.B., Ryan, M.T., Li, X., 2015. A test of the cosmogenic ^{3} He production rate in the south west Pacific (39°S). J. Quat. Sci. 30, 87–97.
Froggatt, P.C., Lowe, D.J., 1990. A review of late Quaternary silicic and some other tephra formations from New Zealand: their stratigraphy, nomenclature, distribution, volume, and age. N. Z. J. Geol. Geophys. 33, 89–109.
Furbish, D.J., Andrews, J.T., 1984. The use of hypsometry to indicate long-term stability and response of valley glaciers to changes in mass transfer. J. Glaciol. 30, 199–211.
Goehring, B.M., Kurz, M.D., Balco, G., Schaefer, J.M., Licciardi, J., Lifton, N., 2010. A reevaluation of in situ cosmogenic ^{3} He production rates. Quat. Geochronol. 5, 410–418.

Golledge, N.R., Mackintosh, A.N., Anderson, B.M., Buckley, K.M., Doughty, A.M., Barrell, D.J.A., Denton, G.H., Vandergoes, M.J., Andersen, B.G., Schaefer, J.M., 2012. Last Glacial Maximum climate in New Zealand inferred from a modelled Southern Alps icefield. Quat. Sci. Rev. 46, 30–45.

Hobden, B.J., Houghton, B.F., Lanphere, M.A., Nairn, I.A., 1996. Growth of the Tongariro volcanic complex: new evidence from K-Ar age determinations. N. Z. J. Geol. Geophys. 39, 151–154.

Hulston, J.R., Lupton, J.E., 1996. Helium isotope studies of geothermal fields in the Taupo Volcanic Zone, New Zealand. J. Volcanol. Geotherm. Res. 74, 297–321.

Ivy-Ochs, S., Kerschner, H., Schlchter, C., 2007. Cosmogenic nuclides and the dating of Lateglacial and Early Holocene glacier variations: the Alpine perspective. Quat. Int. 164165, 53–63.

Kaplan, M.R., Schaefer, J.M., Denton, G.H., Barrell, D.J.A., Chinn, T.J.H., Putnam, A.E., Andersen, B.G., Finkel, R.C., Schwartz, R., Doughty, A.M., 2010. Glacier retreat in New Zealand during the Younger Dryas Stadial. Nature 467, 194–197.

Kaplan, M.R., Schaefer, J.M., Denton, G.H., Doughty, A.M., Barrell, D.J.A., Chinn, T.J.H., Putnam, A.E., Andersen, B.G., Mackintosh, A., Finkel, R.C., et al., 2013. The anatomy of long-term warming since 15 ka in New Zealand based on net glacier snowline rise. Geology 41, 887–890.

Kelley, S.E., Kaplan, M.R., Schaefer, J.M., Andersen, B.G., Barrell, D.J., Putnam, A.E., Denton, G.H., Schwartz, R., Finkel, R.C., Doughty, A.M., 2014. High-precision ^{10}Be chronology of moraines in the Southern Alps indicates synchronous cooling in Antarctica and New Zealand 42,000 years ago. Earth Planet. Sci. Lett. 405, 194–206.

Keys, H., 1988. Survey of the Glaciers on Mt. Ruapehu, Tongariro National Park – a Baseline for Detecting Effects of Climate Change. Department of Conservation, Wellington, NZ, p. 1988. Technical Report Science and Research Internal Report No.24.

Kirkbride, M.P., Dugmore, A.J., 2001. Timing and significance of mid-Holocene glacier advances in northern and central Iceland. J. Quat. Sci. 16, 145–153.

Kuhn, M., 1995. The mass balance of very small glaciers. Z. für Gletscherkd. Glazialgeol. 31, 171–179.

Lal, D., 1991. Cosmic ray labeling of erosion surfaces: in situ nuclide production rates and erosion models. Earth Planet. Sci. Lett. 104, 424–439.

Licciardi, J.M., Clark, P.U., Brook, E.J., Elmore, D., Sharma, P., 2004. Variable responses of western U.S. glaciers during the last deglaciation. Geology 32, 81–84.

Lifton, N., Sato, T., Dunai, T.J., 2014. Scaling *in situ* cosmogenic nuclide production rates using analytical approximations to atmospheric cosmic-ray fluxes. Earth Planet. Sci. Lett. 386, 149–160.

Lifton, N., Smart, D.F., Shea, M.A., 2008. Scaling time-integrated in situ cosmogenic nuclide production rates using a continuous geomagnetic model. Earth Planet. Sci. Lett. 268, 190–201.

Lorrey, A.M., Vandergoes, M., Almond, P., Renwick, J., Stephens, T., Bostock, H., Mackintosh, A., Newnham, R.M., Williams, P.W., Ackerley, D., Neil, H., Fowler, A.M., 2012. Palaeocirculation across New Zealand during the last glacial maximum at 21 ka. Quat. Sci. Rev. 36, 189–213.

Lowe, D.J., Blaauw, M., Hogg, A.G., Newnham, R.M., 2013. Ages of 24 widespread tephras erupted since 30,000 years ago in New Zealand, with re-evaluation of the timing and palaeoclimatic implications of the Lateglacial cool episode recorded at Kaipo bog. Quat. Sci. Rev. 74, 170–194.

Lowe, D.J., Shane, P.A.R., Alloway, B.V., Newnham, R.M., 2008. Fingerprints and age models for widespread New Zealand tephra marker beds erupted since 30,000 years ago: a framework for NZ-INTIMATE. Quat. Sci. Rev. 27, 95–126.

Marden, M., Betts, H., Palmer, A., Taylor, R., Bilderback, E., Litchfield, N., 2014. Post-Last Glacial Maximum fluvial incision and sediment generation in the unglaciated Waipaoa catchment, North Island, New Zealand. Geomorphology 214, 283–306.

Marrero, S.M., Phillips, F.M., Borchers, B., Lifton, N., Aumer, R., Balco, G., 2015. Cosmogenic nuclide systematics and the cronuscalc program. Quat. Geochronol. http://dx.doi.org/10.1016/j.quageo.2015.09.005.

Mathews, W.H., 1967. A contribution to the geology of the Mount Tongariro massif, North Island, New Zealand. N. Z. J. Geol. Geophys. 10, 1027–1038.

McArthur, J.L., Shepherd, M.J., 1990. Late Quaternary glaciation of Mt Ruapehu, North Island, New Zealand, New Zealand. J. R. Soc. N. Z. 20, 287–296.

McCarthy, A., Mackintosh, A., Rieser, U., Fink, D., 2008. Mountain glacier chronology from Boulder Lake, New Zealand, indicates MIS 4 and MIS 2 ice advances of similar extent. Arct. Antarct. Alp. Res. 40, 695–708.

McKinnon, K.A., Mackintosh, A.N., Anderson, B.M., Barrell, D.J.A., 2012. The influence of sub-glacial bed evolution on ice extent: a model-based evaluation of the Last Glacial Maximum Pukaki glacier, New Zealand. Quat. Sci. Rev. 57, 46–57.

Meier, M.F., Post, A.S., 1962. Recent Variations in Mass Net Budgets of Glaciers in Western North America. International Association of Scientific Hydrology Publication, pp. 63–77, 58.

Newnham, R.M., McGlone, M., Moar, N., Wilmshurst, J., Vandergoes, M., 2013. The vegetation cover of New Zealand at the Last Glacial Maximum. Quat. Sci. Rev. 74, 202–214.

Nishiizumi, K., Winterer, E., Kohl, C., Klein, J., Middleton, R., Lal, D., Arnold, J., 1989. Cosmic ray production rates of ^{10}Be and ^{26}Al in quartz from glacially polished rocks. J. Geophys. Res. Solid Earth 1978–2012 (94), 17907–17915.

NIWA, 2014. CliFlo: NIWA's National Climate Database on the Web. Website. http://cliflo.niwa.co.nz/. Retrieved 2014.

Norton, D.A., 1985. A multivariate technique for estimating New Zealand temperature normals. Weather Clim. 5, 64–74.

Oerlemans, J., 1997. Climate sensitivity of Franz Josef Glacier, New Zealand, as revealed by numerical modeling. Arct. Alp. Res. 29, 233–239.

Oerlemans, J., Fortuin, J.P.F., 1992. Sensitivity of glaciers and small ice caps to greenhouse warming. Science 258, 115–117.

Osmaston, H., 2005. Estimates of glacier equilibrium line altitudes by the Area Altitude, the Area Altitude Balance Ratio and the Area Altitude Balance Index methods and their validation. Quat. Int. 138–139, 22–31.

Pahnke, K., Sachs, J.P., 2006. Sea surface temperatures of southern midlatitudes 0–160 kyr BP. Paleoceanography 21, PA2003.

Paterson, W.S.B., 1994. The Physics of Glaciers. Elsevier, Oxford, New York and Tokyo.

Patterson, D., Honda, M., McDougall, I., 1994. Noble gases in mafic phenocrysts and xenoliths from New Zealand. Geochimica Cosmochimica Acta 58, 4411–4427.

Portenga, E.W., Bierman, P.R., 2011. Understanding Earth's eroding surface with ^{10}Be. GSA Today 21, 4–10.

Porter, S.C., 1975. Equilibrium-line altitudes of late Quaternary glaciers in the Southern Alps, New Zealand. Quat. Res. 5, 27–47.

Preusser, F., Andersen, B.G., Denton, G.H., Schlüchter, C., 2005. Luminescence chronology of Late Pleistocene glacial deposits in North Westland, New Zealand. Quat. Sci. Rev. 24, 2207–2227.

Pulford, A.K., 2002. Crustal Structure and Lithospheric Doming: Aspects of Deformation along an Obliquely Convergent Plate Margin, New Zealand. Ph.D. Thesis. Victoria University of Wellington.

Purdie, H., Anderson, B., Chinn, T., Owens, I., Mackintosh, A., Lawson, W., 2014. Franz Josef and Fox Glaciers, New Zealand: historic length records. Glob. Planet. Change 121, 41–52.

Putnam, A.E., Denton, G.H., Schaefer, J.M., Barrell, D.J.A., Andersen, B.G., Finkel, R.C., Schwartz, R., Doughty, A.M., Kaplan, M.R., Schlüchter, C., 2010a. Glacier advance in southern middle-latitudes during the Antarctic Cold Reversal. Nat. Geosci. 3, 700–704.

Putnam, A.E., Schaefer, J.M., Barrell, D.J.A., Vandergoes, M., Denton, G.H., Kaplan, M.R., Finkel, R.C., Schwartz, R., Goehring, B.M., Kelley, S.E., 2010b. In situ cosmogenic ^{10}Be production-rate calibration from the Southern Alps, New Zealand. Quat. Geochronol. 5, 392–409.

Putnam, A.E., Schaefer, J.M., Denton, G.H., Barrell, D.J.A., Andersen, B.G., Koffman, T.N.B., Rowan, A.V., Finkel, R.C., Rood, D.H., Schwartz, R., Vandergoes, M.J., Plummer, M.A., Brocklehurst, S.H., Kelley, S.E., Ladig, K.L., 2013a. Warming and glacier recession in the Rakaia valley, Southern Alps of New Zealand, during Heinrich Stadial 1. Earth Planet. Sci. Lett. 382, 98–110.

Putnam, A.E., Schaefer, J.M., Denton, G.H., Barrell, D.J.A., Birkel, S.D., Andersen, B.G., Kaplan, M.R., Finkel, R.C., Schwartz, R., Doughty, A.M., 2013b. The Last Glacial Maximum at 44°S documented by a ^{10}Be moraine chronology at Lake Ohau, Southern Alps of New Zealand. Quat. Sci. Rev. 62, 114–141.

Putnam, A.E., Schaefer, J.M., Denton, G.H., Barrell, D.J.A., Finkel, R.C., Andersen, B.G., Schwartz, R., Chinn, T.J., Doughty, A.M., 2012. Regional climate control of glaciers in New Zealand and Europe during the pre-industrial Holocene. Nat. Geosci. 5, 627–630.

Rea, B.R., Whalley, W.B., Dixon, T.S., Gordon, J.E., 1999. Plateau icefields as contributing areas to valley glaciers and the potential impact on reconstructed ELAs: a case study from the Lyngen Alps, North Norway. Ann. Glaciol. 28, 97–102.

Roethlisberger, F., Schneebeli, W., 1979. Genesis of lateral moraine complexes, demonstrated by fossil soils and trunks; indicators of postglacial climatic fluctuations. In: Schlüchter, C. (Ed.), Moraines and Varves: Origin, Genesis, Classification. Balkema, Rotterdam, The Netherlands, pp. 387–420.

Rojas, M., Moreno, P., Kageyama, M., Crucifix, M., Hewitt, C., Abe Ouchi, A., Ohgaito, R., Brady, E.C., Hope, P., 2009. The Southern Westerlies during the last glacial maximum in PMIP2 simulations. Clim. Dyn. 32, 525–548.

Rother, H., Fink, D., Shulmeister, J., Mifsud, C., Evans, M., Pugh, J., 2014. The early rise and late demise of New Zealand's last glacial maximum. Proc. Natl. Acad. Sci. 111, 11630–11635.

Rowan, A.V., Plummer, M.A., Brocklehurst, S.H., Jones, M.A., Schultz, D.M., 2013. Drainage capture and discharge variations driven by glaciation in the Southern Alps, New Zealand. Geology 41, 199–202.

Schaefer, J.M., Denton, G.H., Barrell, D.J.A., Ivy Ochs, S., Kubik, P.W., Andersen, B.G., Phillips, F.M., Lowell, T.V., Schlüchter, C., 2006. Near-synchronous interhemispheric termination of the Last Glacial Maximum in mid-latitudes. Science 312, 1510–1513.

Schaefer, J.M., Denton, G.H., Kaplan, M., Putnam, A., Finkel, R.C., Barrell, D.J.A., Andersen, B.G., Schwartz, R., Mackintosh, A., Chinn, T., Schlüchter, C., 2009. High-frequency Holocene glacier fluctuations in New Zealand differ from the northern signature. Science 324, 622–625.

Schaefer, J.M., Putnam, A.E., Denton, G.H., Kaplan, M.R., Birkel, S., Doughty, A.M., Kelley, S., Barrell, D.J.A., Finkel, R.C., Winckler, G., Anderson, R.F., Ninneman, U.S., Barker, S., Schwartz, R., Schlüchter, C., 2015. The Southern Glacial Maximum 65000 years ago and its Unfinished Termination. Quat. Sci. Rev. 114, 52–60.

Seltzer, A., Stute, M., Morgenstern, U., Stewart, M., Schaefer, J., 2015. Mean annual temperature in new zealand during the last glacial maximum derived from dissolved noble gases in groundwater. Earth Planet. Sci. Lett. 431, 206–216.

Shane, P., 2000. Tephrochronology: a New Zealand case study. Earth Sci. Rev. 49, 223–259.

Shane, P., Nairn, I.A., Martin, S.B., Smith, V.C., 2008. Compositional heterogeneity in tephra deposits resulting from the eruption of multiple magma bodies: implications for tephrochronology. Quat. Int. 178, 44–53.

Shane, P., Sandiford, A., 2003. Paleovegetation of marine isotope stages 4 and 3 in Northern New Zealand and the age of the widespread Rotoehu tephra. Quat. Res. 59, 420–429.

Shulmeister, J., Shane, P., Lian, O.B., Okuda, M., Carter, J.A., Harper, M., Dickinson, W., Augustinus, P., Heijnis, H., 2001. A long late-Quaternary record from Lake Poukawa, Hawkes Bay, New Zealand. Palaeogeogr. Palaeoclimatol. Palaeoecol. 176, 81–107.
Sikes, E.L., Howard, W.R., Samson, C.R., Mahan, T.S., Robertson, L.G., Volkman, J.K., 2009. Southern ocean seasonal temperature and subtropical front movement on the South Tasman Rise in the Late Quaternary. Paleoceanography 24, PA2201.
Stephens, T., Atkin, D., Cochran, U., Augustinus, P., Reid, M., Lorrey, A., Shane, P., Street Perrott, A., 2012. A diatom-inferred record of reduced effective precipitation during the Last Glacial Coldest Phase (28.8–18.0 cal kyr BP) and increasing Holocene seasonality at Lake Pupuke, Auckland, New Zealand. J. Paleolimnol. 48, 801–817.
Stone, J.O., 2000. Air pressure and cosmogenic isotope production. J. Geophys. Res. B Solid Earth 105, 23753–23759.
Sturman, A.P., Tapper, N.J., 1996. The Weather and Climate of Australia and New Zealand. Oxford University Press, Melbourne, Australia.
Suganuma, Y., Miura, H., Okuno, J., 2012. A new sampling technique for surface exposure dating using a portable electric rock cutter. Antarct. Rec. 56, 85–90.
Suggate, R.P., 1990. Late Pliocene and quaternary glaciations of New Zealand. Quat. Sci. Rev. 9, 175–197.
Suggate, R.P., Almond, P.C., 2005. The Last Glacial Maximum (LGM) in western South Island, New Zealand: Implications for the global LGM and MIS 2. Quat. Sci. Rev. 24, 1923–1940.
Sutherland, R., Kim, K., Zondervan, A., McSaveney, M., 2007. Orbital forcing of mid-latitude Southern Hemisphere glaciation since 100 ka inferred from cosmogenic nuclide ages of moraine boulders from the Cascade Plateau, southwest New Zealand. Bull. Geol. Soc. Am. 119, 443–451.
Sutton, P.J.H., Bowen, M., Roemmich, D., 2005. Decadal temperature changes in the Tasman Sea. N. Z. J. Mar. Freshw. Res. 39, 1321–1329.
Topping, W.W., 1974. Some Aspects of Quaternary History of Tongariro Volcanic Centre. Ph.D. Thesis. Victoria University of Wellington.
Topping, W.W., Kohn, B.P., 1973. Rhyolitic tephra marker beds in the Tongariro area, North Island, New Zealand. N. Z. J. Geol. Geophys. 16, 375–395.
Torgersen, T., Lupton, J., Sheppard, D., Giggenbach, W., 1982. Helium isotope variations in the thermal areas of New Zealand. J. Volcanol. Geotherm. Res. 12, 283–298.
Uddstrom, M.J., Oien, N.A., 1999. On the use of high-resolution satellite data to describe the spatial and temporal variability of sea surface temperatures in the New Zealand region. J. Geophys. Res. C Oceans 104, 20729–20751.
Vandergoes, M.J., Hogg, A.G., Lowe, D.J., Newnham, R.M., Denton, G.H., Southon, J., Barrell, D.J.A., Wilson, C.J.N., McGlone, M.S., Allan, A.S.R., Almond, P.C., Petchey, F., Dabell, K., Dieffenbacher Krall, A.C., Blaauw, M., 2013. A revised age for the Kawakawa/Oruanui tephra, a key marker for the Last Glacial Maximum in New Zealand. Quat. Sci. Rev. 74, 195–201.
Whittaker, T.E., Hendy, C.H., Hellstrom, J.C., 2011. Abrupt millennial-scale changes in intensity of Southern Hemisphere westerly winds during marine isotope stages 2–4. Geology 39, 455–458.
Williams, P.W., 1996. A 230 ka record of glacial and interglacial events from Aurora Cave, Fiordland, New Zealand. N. Z. J. Geol. Geophys. 39, 225–241.
Williams, P.W., McGlone, M., Neil, H., Zhao, J.X., 2015. A review of New Zealand palaeoclimate from the Last Interglacial to the global Last Glacial Maximum. Quat. Sci. Rev. 110, 92–106.
Winckler, G., Anderson, R.F., Schlosser, P., 2005. Equatorial Pacific productivity and dust flux during the mid-Pleistocene climate transition. Paleoceanography 20, PA4025.